NATIONAL ADVISORY COMMITTEE FOR AERONAUTICS

TECHNICAL NOTE 3551

EXPERIMENTAL INVESTIGATION AT LOW SPEED OF EFFECTS OF FUSELAGE CROSS SECTION ON STATIC LONGITUDINAL AND LATERAL STABILITY CHARACTERISTICS OF MODELS HAVING 0° AND 45° SWEPTBACK SURFACES

By William Letko and James L. Williams

Langley Aeronautical Laboratory
Langley Field, Va.

Washington
December 1955

NATIONAL ADVISORY COMMITTEE FOR AERONAUTICS

TECHNICAL NOTE 3551

EXPERIMENTAL INVESTIGATION AT LOW SPEED OF EFFECTS OF FUSELAGE CROSS SECTION ON STATIC LONGITUDINAL AND LATERAL STABILITY CHARACTERISTICS OF MODELS HAVING 0° AND 45° SWEPTBACK SURFACES

By William Letko and James L. Williams

SUMMARY

An experimental investigation at low speed was made to determine the effects of fuselage cross section on the static longitudinal and lateral stability characteristics of midwing airplane models having 0° and 45° sweptback surfaces. The results indicated that the main effects of fuselage cross section on the longitudinal and directional stability characteristics of the models at low angles of attack are caused by the direct contributions of the fuselage. At the high angles of attack, in addition to the direct contributions of the fuselage, wing-fuselage interference (sidewash) with the tail decreases the tail contributions to the directional stability. The configuration consisting of the wing and deep fuselage produced the most detrimental effect, and the configuration consisting of the wing and shallow fuselage was the least detrimental in this respect. For the complete configurations tested, fuselage cross section had little effect on the range of linearity of the curves of yawing moment against sideslip angle for the angles of attack and sideslip investigated. In general, the configuration with the deep fuselage had the poorest directional characteristics of the models investigated.

INTRODUCTION

Most of the main components of airplanes have undergone design changes in order to meet the demands of high-speed flight; not the least of these is the airplane fuselage. Various jet-engine installations in fuselages and in wing-fuselage junctures have resulted in a variety of fuselage cross-sectional shapes. Although there are numerous data on configurations with bodies of circular cross section such as those presented in references 1, 2, and 3, little data of systematic nature are available for other shapes.

In order to provide data on the effect of fuselage cross section on airplane static longitudinal and lateral stability characteristics, several fuselages with interchangeable wing and tail surfaces have been tested in the Langley stability tunnel. The fuselages tested were of round, square, and rectangular cross sections. The fuselages of square and rectangular cross sections had rounded corners. The wings and tails tested successively on the fuselages had 0° and 45° sweepback. All the configurations were tested with the wing in the midwing location. Presented herein are the static longitudinal and lateral stability characteristics of these configurations.

SYMBOLS

The data presented are referred to the stability system of axes with the origin at the projection on the plane of symmetry of the calculated aerodynamic center of the wing. Positive directions of forces, moments, and angular displacements are shown in figure 1. The coefficients and symbols are defined as follows:

C_L	lift coefficient, L/qS_W
C_D	drag coefficient, D/qS_W
C_Y	lateral-force coefficient, F_Y/qS_W
C_l	rolling-moment coefficient, M_X/qS_Wb_W
C_m	pitching-moment coefficient, $M_Y/qS_W\bar{c}_W$
C_n	yawing-moment coefficient, M_Z/qS_Wb_W
L	lift
D	drag
F_Y	lateral force
M_X	rolling moment
M_Y	pitching moment
M_Z	yawing moment

q	dynamic pressure, $\frac{1}{2}\rho V^2$
V	free-stream velocity
ρ	mass density of air
A	aspect ratio, b^2/S
b	span, measured perpendicular to fuselage center line
S	surface area
c	chord, measured parallel to plane of symmetry
c_r	root chord
c_t	tip chord
$\bar{c}$	mean aerodynamic chord; for example, $\bar{c}_W = \frac{2}{S_W}\int_0^{b_W/2} c_W^2 dy$
y	coordinate along Y-axis, measured from plane of symmetry
l_V or l_H	tail length, distance parallel to fuselage center line from mounting point to $\bar{c}_V/4$ or $\bar{c}_H/4$
h	perpendicular distance from fuselage center line to $\bar{c}_V/4$ (tail root chord coincides with fuselage center line)
R	ordinate of circular fuselage
r	fuselage corner radius, $R/3$
w	local half-width of square or rectangular fuselage
d	local half-depth of square or rectangular fuselage; for square fuselage, $d = w$
x	longitudinal distance along fuselage center line
λ	taper ratio, c_t/c_r
Λ	angle of sweepback of quarter-chord line, deg
β	angle of sideslip, deg

ψ azimuth angle, deg

α angle of attack, deg

$C_{Y_\beta} = \frac{\partial C_Y}{\partial \beta}$

$C_{n_\beta} = \frac{\partial C_n}{\partial \beta}$

$C_{l_\beta} = \frac{\partial C_l}{\partial \beta}$

ΔC_{Y_β}, ΔC_{n_β} contribution of the tail group to derivatives; that is, for the wing on,

$$\Delta C_{Y_\beta} = \left(C_{Y_\beta}\right)_{W+F+V+H} - \left(C_{Y_\beta}\right)_{W+F}$$

for the wing off,

$$\Delta C_{Y_\beta} = \left(C_{Y_\beta}\right)_{F+V+H} - \left(C_{Y_\beta}\right)_{F}$$

and for a wing-tail configuration,

$$\Delta C_{Y_\beta} = \left(C_{Y_\beta}\right)_{W+V+H} - \left(C_{Y_\beta}\right)_{W}$$

Subscripts and abbreviations:

F fuselage; used with subscripts 1 to 4 to denote various fuselages (see fig. 2)

H horizontal tail; used with subscripts 1 and 2 (see fig. 3)

V vertical tail; used with subscripts 1 to 6 to denote various vertical tails (see figs. 3 and 4)

W wing; used with subscripts 1 and 2 (see fig. 3)

APPARATUS AND MODELS

The tests were conducted in the 6- by 6-foot test section of the Langley stability tunnel.

The models were designed to permit tests of the wing alone, the fuselage alone, the wing-fuselage combination, or the fuselage with any tail configuration with or without the wings. Drawings of the component parts of the models tested are given in figures 2 to 4 and in table I. A side view, cross section, and designation of each fuselage is given in figure 2. The coordinates of the circular-cross-section fuselage are given in table I. The coordinates of the square and rectangular fuselages were determined so that the variation of the cross-sectional area of each fuselage along the longitudinal axis was the same as that of the circular fuselage. The equations used to determine the coordinates of the square and rectangular fuselages are given in table I. The rectangular fuselage was tested both with the major cross-sectional axis vertical (fuselage 3) and with the major axis horizontal (fuselage 4). (See fig. 2.)

The configurations had both swept and unswept wing and tail surfaces. The quarter-chord lines were swept back 0° and 45° for the unswept and sweptback surfaces, respectively. The wings had a taper ratio of 0.6 and an aspect ratio of 4. The tail surfaces also had a taper ratio of 0.6. The aspect ratio and other geometric characteristics of the various tail surfaces as well as those of the wings can be found in table II. Drawings showing the geometric characteristics of the wing and tail surfaces are given as figures 3 and 4. All the configurations were tested with the wing in the midwing location. All lifting surfaces were set at 0° incidence with respect to the fuselage center line.

The models were mounted on a single strut support at the quarter-chord point of the wings which were located with respect to the fuselage and tail surfaces as shown in figure 5. For tests of the complete-model and fuselage-tail configurations, the vertical tail was mounted so that the vertical-tail root-chord line coincided with the fuselage center line.

For the wing-tail configurations, the tail was mounted at an appropriate tail length on a steel tube of small diameter which was fastened to the wing. The isolated tail was mounted on the same tube which was then attached to the model support strut. For the wing-tail and isolated-tail tests, the tail area included the portion normally enclosed in the fuselage.

Forces and moments were measured by means of a conventional six-component mechanical balance system.

TESTS AND CORRECTIONS

Tests were made at a dynamic pressure of 24.9 pounds per square foot, which corresponds to a Mach number of about 0.13 and a Reynolds number of about 0.71×10^6 based on the mean aerodynamic chord of the wings. The models were tested through an angle-of-attack range from -4° up to and beyond maximum lift (of wings alone) at angles of sideslip of 0° and $\pm 5^\circ$. Tests of the complete configurations were also made at angles of attack of 0°, 10°, 20°, and 26° through a sideslip range from -20° to 20°.

Approximate corrections based on unswept-wing theory for the effects of jet boundaries (ref. 4) have been applied to the lift, drag, and pitching-moment coefficients. No corrections have been applied to the data for the effects of blockage or support-strut interference.

RESULTS AND DISCUSSION

Presentation of Results

The static longitudinal stability characteristics of the models are given in figures 6 to 10, and the static lateral stability characteristics are presented in figures 11 to 26. A summary of the configurations investigated and of the figures that present the basic data for these configurations is given in table III.

Static Longitudinal Stability Characteristics

Complete model.- The static longitudinal stability characteristics of the complete configurations are given in figure 6. In the low angle-of-attack range the square- and circular-fuselage configurations have about the same stability and are more stable than the configuration with the shallow fuselage (fuselage 4) and less stable than the configuration with the deep fuselage (fuselage 3). At angles of attack above 8° and below about 18° there is a large increase in the stability of all the unswept configurations and a large decrease in the stability of all the swept configurations regardless of fuselage cross section. At angles of attack above 18° the reverse is true in that a large decrease in stability occurs for the unswept configurations and, with the exception of the configuration with fuselage 4, a large increase in stability occurs for the swept configurations.

Although the horizontal tail for the unswept configurations generally does not provide adequate stability at low angles of attack for the center-of-gravity positions used, the main purpose of the paper, which is

to provide an indication of the effects of fuselage cross section, is not affected.

Differences caused by body cross section on the lift and drag are generally small at low angles of attack but become larger at the high angles of attack. The configuration with the shallow fuselage (fuselage 4) has the highest lift and drag at the high angles of attack. The reason for the low values of drag coefficient up to an angle of attack of 8° for the complete configuration with fuselage 3 is not clear since the data for the wing-fuselage combination do not show this effect (fig. 7).

Wing-fuselage configuration.- In general, the comments concerning the static longitudinal stability characteristics for the complete model also apply to the wing-fuselage configurations. (See fig. 7.)

Fuselage and fuselage-tail configurations.- In figures 8 and 9 are presented the static longitudinal stability characteristics of the fuselage and fuselage-tail configurations. There are two sets of pitching-moment data for the fuselage alone since the center of gravity was slightly different when the fuselage was used in conjunction with swept and unswept wing-tail surfaces. This difference in center-of-gravity location caused only a small difference in the longitudinal stability of the fuselages. (See fig. 8.) The fuselages are a little more unstable with the center-of-gravity location used for the swept configurations (rearward location) than for the center-of-gravity location used with the unswept configurations.

The effect of cross section is, of course, the same for both center-of-gravity locations with the shallow fuselage (fuselage 4) being the most unstable and the deep fuselage (fuselage 3) generally being the least unstable. At low angles of attack there is little difference in the longitudinal stability obtained for the circular and square fuselages; however, the unstable contribution of the circular fuselage is less at the high angles of attack than that of the square fuselage. The shallow fuselage (fuselage 4) has the highest lift and drag at the high angles of attack.

Adding the tail unit to the fuselages results, of course, in stable pitching-moment curves at the low angles of attack (fig. 9). The configuration with shallow fuselage and tail is the least stable. For all fuselages and for the unswept tail, the slope of the curves of C_m plotted against α is practically zero at the high angles of attack for the test center-of-gravity position.

Wing, tail, and wing-tail configurations.- The longitudinal stability characteristics of the wing, isolated tail, and wing-tail configurations are given in figure 10. The details pertaining to the mounting of the

tail for the wing-tail and isolated-tail tests are given in the section entitled "Apparatus and Models."

The swept and unswept wings used in the present investigation have been reported on in several other investigations such as references 5, 6, and 7, and there is little need, here, to discuss in detail the characteristics of the wings.

Figure 10 shows that adding the wing to the isolated tail causes a decrease in longitudinal stability at low angles of attack which is much larger for the unswept wing than that obtained with the swept-wing configuration. The decrease in longitudinal stability obtained is caused by wing downwash. For both the swept and unswept configurations, the general variation of pitching-moment coefficient with angle of attack for the wing-tail configuration is very similar to the variation obtained for the complete configurations. For the complete configurations there is, of course, a difference in initial slopes at low angles of attack, mainly because the unstable contribution of the fuselage varies with the fuselage cross section.

Static Lateral Stability Characteristics

Complete model.- The static lateral stability derivatives C_{Y_β}, C_{l_β}, and C_{n_β} (obtained from data at $\beta = \pm 5^\circ$) for the complete model configurations are given in figure 11. For both the swept and unswept models, there is little difference in the values of C_{n_β} for the configurations with the circular or square fuselage at low angles of attack. However, the values of C_{n_β} obtained for the configurations with shallow fuselage (fuselage 4) were appreciably greater (indicating greater directional stability), and the values of C_{n_β} for the deep-fuselage configuration were appreciably less than those obtained for the circular- and square-fuselage configurations. This difference in the values of C_{n_β} at the low angles of attack can be attributed mainly to the difference in the fuselage contributions. Except for the deep-fuselage configuration $\left(W_1 + F_3 + V_1 + H_1\right)$, the values of C_{n_β} are positive and fairly constant throughout the angle-of-attack range for the unswept models. The values of C_{n_β} for the deep-fuselage configuration are positive up to an angle of attack of about 20° after which C_{n_β} becomes negative. The swept configurations have positive and nearly constant values of C_{n_β} throughout the low angles of attack. For all fuselage configurations, C_{n_β} becomes negative at the higher angles of attack and remains negative for

the test angle-of-attack range except for the square-fuselage configuration which has positive values of C_{n_β} above an angle of attack of about 27°. The values of C_{n_β} for the configurations with the deep fuselage become negative at an angle of attack of only 3°. It should be pointed out that, although the values of C_{n_β} for the circular and square configurations are nearly the same at low angles of attack, they differ appreciably at higher angles of attack for the swept models.

As was already mentioned, the difference in the values of C_{n_β} at low angles of attack is due mainly to the different contributions of the fuselages. This is illustrated clearly in figure 12, which presents ΔC_{n_β} (the increment due to the tail) obtained by subtracting the value of C_{n_β} for the wing-fuselage combination from the value of C_{n_β} for the complete configuration. For comparison purposes, the values of C_{n_β} for the isolated-tail group are also presented. From figure 12 it can be seen that, generally, the fuselage cross section does not affect the tail contribution to C_{n_β} appreciably except at angles of attack above about 10°. The large differences between the values of ΔC_{n_β} for the complete configurations and the values of C_{n_β} for the isolated tail at angles of attack above 10° illustrate the large interference effects (due to sidewash) of the wing and fuselage on the vertical-tail contribution to C_{n_β}. Generally, the interference effects appear to be larger for the unswept configuration.

In order to illustrate better the effects of fuselage cross section on the variation of C_{n_β} with angle of attack for the complete configurations, additional tails were designed so that the values of C_{n_β} for the deep- and shallow-fuselage configurations would be more nearly equal to those obtained at zero angle of attack for the configurations of round- and square-cross-section fuselages. The required tail sizes of the modified tails were estimated by currently available procedures with the aid of references 8 and 9. The values of C_{Y_β}, C_{l_β}, and C_{n_β} for the deep- and shallow-fuselage configurations with the redesigned vertical tails are compared with the square-fuselage configuration having the original tail in figure 13. From the data for the unswept configuration it can be seen that, even though the values of C_{n_β} for all configurations are nearly the same at zero angle of attack, the values of C_{n_β} still become negative for the configuration with the deep fuselage; however, the angle of attack at which C_{n_β} changes sign is increased from about 20.5° to 24.5°. For the swept configurations (fig. 13(b)), the redesigned tails

decrease the angle of attack at which C_{n_β} becomes negative for the shallow-fuselage configuration, and increase the angle of attack for the deep-fuselage configuration so that the angle of attack at which $C_{n_\beta} = 0$ is nearly the same as that obtained with the original tail and square-fuselage configuration.

The curves of C_{l_β} (fig. 11) show that generally the effect of fuselage cross section on C_{l_β} of the complete configurations is small. Up to an angle of attack of about 4°, the values of C_{l_β} increase more rapidly with angle of attack for the swept configuration than for the unswept configuration as was expected since C_{l_β} depends mainly on the wing geometry.

The values of C_{Y_β} for the deep-fuselage configuration (fuselage 3) are generally more negative at low angles of attack than those obtained with the other configurations tested and become much more negative at the high angles of attack in contrast to the values for the circular-fuselage configuration which become less negative with angle of attack. (See fig. 11.) This holds true for both the swept and unswept configurations. At the high angles of attack, fuselage cross section has a very large effect on C_{Y_β} of the models tested. The changes in tail size caused, of course, greater differences in the values of C_{Y_β} obtained for the different configurations at low angles of attack (fig. 13).

The values of C_{Y_β}, C_{l_β}, and C_{n_β} discussed up to this point were obtained from the values of the coefficients at $\beta = \pm 5^\circ$. In order to show for which range of angle of sideslip these values would apply, figures 14 to 17 are presented and show the variation of C_Y, C_l, and C_n for angles of attack of 0°, 10°, 20°, and 26° for a range of angle of sideslip β from -20° to 20°. For the unswept configuration, the variation of C_Y, C_n, and C_l with β is nonlinear, even at an angle of attack of 0°, with the curve of C_n maintaining its initial slope for a smaller range of angle of sideslip than the curves for C_Y and C_l. The range of sideslip angle for which C_{n_β} remains constant is decreased from -10° to 10° at an angle of attack of 0° to roughly -5° to 5° at an angle of attack of 26°. Although the initial slopes (slopes near $\beta = 0^\circ$) of the curves differ because of fuselage cross section, the range of linearity, with some unimportant exceptions, is not affected appreciably by cross section. This is especially true for C_n. For the swept configurations at zero angle of attack, the variation of C_Y, C_n, and C_l with angle of sideslip is linear for nearly the entire sideslip range tested. For

the higher angles of attack, the curves of C_Y, C_l, and C_n generally become more nonlinear. For the angles of attack of 20° and 26°, of course, the variation of C_n with β is unstable even near $\beta = 0°$. As was the case with the unswept configurations, there appears to be little significant influence of the body cross section on the range of linearity of the curves even though the initial slopes, near $\beta = 0°$, vary because of fuselage cross section.

Wing-fuselage configurations.- The variations of C_{Y_β}, C_{l_β}, and C_{n_β} for the wing-fuselage configurations are given in figure 18. The values of C_{n_β} are nearly constant negative values up to an angle of attack of approximately 12° for both the swept and unswept configurations. At low angles of attack the effects of fuselage cross section on C_{n_β} are about the same as those obtained for the complete configurations. At the higher angles of attack for the unswept configurations, C_{n_β} became positive except for the deep-fuselage configuration. This increase in directional stability with angle of attack for the unswept-wing—fuselage configuration is canceled, more or less, by the increase with angle of attack of the wing-fuselage interference with the tail (fig. 12); and, as was noted earlier, the values of C_{n_β} for the complete configuration remain positive and nearly constant throughout the test angle-of-attack range (fig. 11). The values of C_{n_β} for the swept-wing—fuselage configuration do not become positive for the angle-of-attack range tested except for the square-fuselage configuration which has positive values of C_{n_β} for a small range at high angles of attack.

The variation of C_{l_β} with angle of attack is similar to that obtained for the complete configuration, since C_{l_β} depends mainly on the wing characteristics. The effect of fuselage cross section on C_{l_β} is small for both the swept and unswept configurations in the low angle-of-attack range but becomes somewhat larger at the higher angles of attack. As was noted for the complete configurations, C_{Y_β} becomes very large at the higher angles of attack for the deep-fuselage configuration, and the effects of fuselage cross section on C_{Y_β} are very large at these angles of attack.

Fuselage and fuselage-tail configuration.- The variation with angle of attack of C_{Y_β}, C_{l_β}, and C_{n_β} for the fuselages is shown in figure 19. Data are presented for two center-of-gravity locations; one location corresponds to the center-of-gravity position for the unswept configurations and the other to the center-of-gravity position used for the

swept configuration. The fuselage with the more rearward center-of-gravity position (used with the swept configurations) is slightly more unstable directionally than that with the forward center-of-gravity location. At low angles of attack, the shallow fuselage (fuselage 4) is least unstable directionally, whereas the deep fuselage has the greatest directional instability. The effect of fuselage cross section on C_{n_β} varies considerably with angle of attack, and although the values of C_{n_β} for the square and circular fuselage are nearly the same at low angles of attack, there is a large difference at the higher angles of attack. The same effects are observed for C_{Y_β}.

At the high angles of attack, relatively large values of C_{Y_β} are obtained for the deep fuselage (fuselage 3) as was the case for configurations with the deep fuselage discussed in previous sections. Also, rather high values of C_{Y_β} are obtained for the square fuselage.

For the fuselage-tail configurations, C_{n_β} is positive in the low angle-of-attack range for all fuselage configurations; however, C_{n_β} remains positive through the entire angle-of-attack range tested only for the circular-fuselage configuration. (See fig. 20.) The deep-fuselage configuration is the least stable initially, and the values of C_{n_β} become negative at a lower angle of attack for this configuration than for the other configurations. This angle of attack is only 4° for the swept configuration. Both the square- and deep-fuselage configurations have large negative values of C_{Y_β} at high angles of attack.

The wing-off interference or sidewash effects of the fuselage on the tail contribution to C_{n_β} are illustrated in figure 21. Here the tail increment ΔC_{n_β} obtained by subtracting the value of C_{n_β} for the fuselage from the value of C_{n_β} of the fuselage-tail group combination is plotted against angle of attack. Also plotted in figure 21 is the C_{n_β} contribution of the isolated tail. The interference effects up to an angle of attack of approximately 10° are generally small and there is little effect of cross section on the interference in this range. At the higher angles of attack, comparison of the tail-contribution increments of the various configurations with the isolated-tail results indicates that the circular fuselage has beneficial interference effects for both swept and unswept tails. The effects of deviating from the circular cross section are for the most part detrimental interference (sidewash) effects which are generally large but vary with angle of attack. These sidewash effects are modified, of course, when the wing is added. (See fig. 12.) In regard to the tail increment ΔC_{n_β}, the results obtained in reference 10 are of interest. The data of reference 10, which were

obtained at an angle of attack of 32°, show a positive increment of C_{n_β} for an unswept tail tested on a flat fuselage with major axes vertical and a negative increment for a flat fuselage with major axes horizontal. This result is the same as that obtained at an angle of attack of 32° in the present investigation for fuselages 3 and 4, respectively (fig. 21); however, as can be seen from figure 21, the tail increment varies considerably with angle of attack, and at some angles of attack the results are opposite those obtained at an angle of attack of 32°.

Wing, tail, and wing-tail configurations.- The variation with angle of attack of C_{Y_β}, C_{l_β}, and C_{n_β} for the wing, isolated-tail, and wing-tail configurations is presented in figure 22. From a study of this figure it can be concluded that the wing, whether swept or unswept, decreases the tail contribution to C_{n_β} of the wing-tail configuration at the higher angles of attack. For the unswept wing, however, the values of C_{n_β} for the wing itself are positive at the higher angles of attack and approximately equal to the interference effect so that, for the unswept-wing—tail configuration, the values of C_{n_β} remain virtually constant throughout the angle-of-attack range tested. For the swept configuration, the negative values of C_{n_β} for the wing itself and the wing interference with the tail result in a decrease in effectiveness and, indeed, a negative C_{n_β} contribution of the tail group at some of the high angles of attack.

For comparison purposes, increments in C_{n_β} and C_{Y_β} contributed by the tail when the tail was tested in combination with the wing-fuselage configuration, the wing (fuselage off), and with the fuselage (wing off) are presented in figures 23 to 26. The increments contributed to C_{n_β} by the tail when tested in combination with the wing and fuselage, for example, were obtained by subtracting the value of C_{n_β} obtained for the wing-fuselage configuration from that obtained for the complete configuration $\left(C_{n_\beta}\right)_{W+F+V+H} - \left(C_{n_\beta}\right)_{W+F}$. Also presented in the figures are the values of C_{n_β} obtained with the isolated tail tested, of course, at the proper tail length. The approximate angle of attack for maximum lift coefficient for each wing is also indicated in figures 23 to 26. A study of these figures indicates that the separate effects of the wing and fuselage on the tail contribution to C_{n_β} at the high angles of attack are not additive but are modified when the wing and fuselage are combined. The effects depend somewhat on the wing sweep and on fuselage cross section. It should be noted that, even though the wing-off fuselage-tail interference effects at high angles of attack for the circular-fuselage configuration are such as to increase the tail effectiveness, addition of the wing results in

interference effects which greatly reduce the tail contribution to C_{n_β} at these angles.

CONCLUSIONS

An investigation at low speed to determine the effects of fuselage cross section on the static longitudinal and lateral stability characteristics of midwing airplane models was made through an angle-of-attack range from -4° up to and beyond maximum lift (of wings alone) at angles of sideslip of 0° and $\pm 5^\circ$. Some tests were also made at angles of attack of 0°, 10°, 20°, and 26° through a sideslip range from -20° to 20°. The results of the investigation indicated the following conclusions:

1. The main effect of fuselage cross section on the static longitudinal stability of models at low angles of attack is due to the direct fuselage contribution, the shallow fuselage being the most destabilizing. Generally, at the high angles of attack there is little significant difference caused by fuselage cross section in the variation of pitching moment with angle of attack for the different configurations.

2. The main effect of fuselage cross section on the directional stability of the models at low angles of attack is due to the direct contribution of the fuselage. The deep-fuselage contribution is the most destabilizing and the shallow-fuselage contribution is the least destabilizing.

3. Wing-fuselage interference (sidewash) with the tail decreases the tail contribution to directional stability at the high angles of attack with the deep-fuselage—wing interference producing the most detrimental effect and the shallow-fuselage—wing interference being the least detrimental in this respect. Wing-off interference effects of the circular-cross-section fuselage on the tail are beneficial at the high angles of attack. Deviating from the circular cross section results generally in large detrimental effects which vary with angle of attack and which are larger than the combined wing-fuselage interference effects for some angles of attack.

4. Except for the deep-fuselage configurations, the complete unswept configurations have positive and nearly constant directional stability through the angle-of-attack range because the direct wing-fuselage contribution to directional stability is positive at the high angles of attack and compensates for the effects of sidewash. No like compensating effect occurs for the swept configurations, and the directional stability becomes negative at some angle of attack that depends on fuselage cross section.

5. For the complete configurations tested, fuselage cross section has little effect on the range of linearity of the curves of yawing moment against sideslip angle up to the maximum angle of attack investigated (26°).

6. In general, the configurations with the deep fuselage have the poorest directional characteristics of the models investigated. At large angles of attack, the deep-fuselage configurations, when at an angle of sideslip, had relatively large values of side force in addition to an unstable variation of yawing-moment coefficient with sideslip angle.

Langley Aeronautical Laboratory,
National Advisory Committee for Aeronautics,
Langley Field, Va., September 9, 1955.

REFERENCES

1. Queijo, M. J., and Wolhart, Walter D.: Experimental Investigation of the Effect of Vertical-Tail Size and Length and of Fuselage Shape and Length on the Static Lateral Stability Characteristics of a Model With 45° Sweptback Wing and Tail Surfaces. NACA Rep. 1049, 1951. (Supersedes NACA TN 2168.)

2. Wolhart, Walter D.: Influence of Wing and Fuselage on the Vertical-Tail Contribution to the Low-Speed Rolling Derivatives of Midwing Airplane Models With 45° Sweptback Surfaces. NACA TN 2587, 1951.

3. Letko, William: Effect of Vertical-Tail Area and Length on the Yawing Stability Characteristics of a Model Having a 45° Sweptback Wing. NACA TN 2358, 1951.

4. Silverstein, Abe, and White, James A.: Wind-Tunnel Interference With Particular Reference to Off-Center Positions of the Wing and to the Downwash at the Tail. NACA Rep. 547, 1936.

5. Letko, William, and Riley, Donald R.: Effect of an Unswept Wing on the Contribution of Unswept-Tail Configurations to the Low-Speed Static- and Rolling-Stability Derivatives of a Midwing Airplane Model. NACA TN 2175, 1950.

6. Brewer, Jack D., and Lichtenstein, Jacob H.: Effect of Horizontal Tail on Low-Speed Static Lateral Stability Characteristics of a Model Having 45° Sweptback Wing and Tail Surfaces. NACA TN 2010, 1950.

7. Goodman, Alex: Effects of Wing Position and Horizontal-Tail Position on the Static Stability Characteristics of Models With Unswept and 45° Sweptback Surfaces With Some Reference to Mutual Interference. NACA TN 2504, 1951.

8. DeYoung, John, and Harper, Charles W.: Theoretical Symmetric Span Loading at Subsonic Speeds for Wings Having Arbitrary Plan Form. NACA Rep. 921, 1948.

9. Queijo, M. J., and Riley, Donald R.: Calculated Subsonic Span Loads and Resulting Stability Derivatives of Unswept and 45° Sweptback Tail Surfaces in Sideslip and in Steady Roll. NACA TN 3245, 1954.

10. Bates, William R.: Static Stability of Fuselages Having a Relatively Flat Cross Section. NACA TN 3429, 1955. (Supersedes NACA RM L9I06a.)

TABLE I.- COORDINATES OF THE CIRCULAR-CROSS-SECTION FUSELAGE AND EQUATIONS FOR COORDINATES OF THE SQUARE- AND RECTANGULAR-CROSS-SECTION FUSELAGES

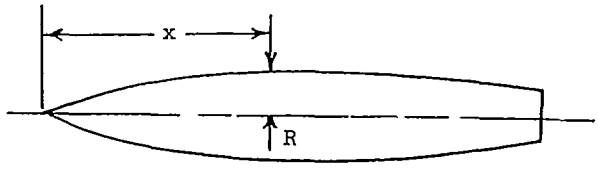

Circular-fuselage coordinates

x, in.	R, in.
0	0
2	.64
4	1.20
6	1.68
8	2.09
10	2.42
12	2.67
14	2.85
16	2.96
18	3.00
20	2.99
22	2.97
24	2.93
26	2.87
28	2.79
30	2.70
32	2.60
34	2.47
36	2.33
38	2.18
40	2.01
42	1.82
44	1.61
45	1.50

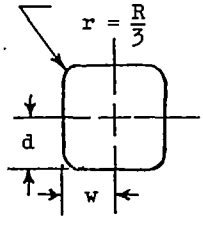

Equation for coordinates of square fuselage:

$$4w^2 - 4\left(\frac{R}{3}\right)^2 - \pi\left(\frac{R}{3}\right)^2 = \pi R^2$$

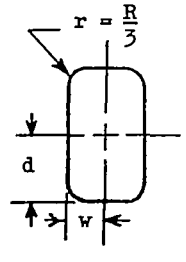

Equations for coordinates of rectangular fuselage:

$$4wd - 4\left(\frac{R}{3}\right)^2 - \pi\left(\frac{R}{3}\right)^2 = \pi R^2$$

$$w = \frac{2}{3}R$$

TABLE II.- PERTINENT GEOMETRIC CHARACTERISTICS OF MODEL

	W_1	W_2
Wing:		
Aspect ratio, A_W	4	4
Taper ratio, λ_W	0.6	0.6
Quarter-chord sweep angle, Λ, deg	0	45
Dihedral angle, deg	0	0
Twist, deg	0	0
NACA airfoil section	65A008	65A008
Area, S_W, sq in.	324	324
Span, b_W, in.	36	36
Mean aerodynamic chord, $\bar{c}_W$, in.	9.19	9.19

	V_1	V_2	V_3	V_4	V_5	V_6
Vertical tail:						
Aspect ratio, A_V	2	1.4	2	2	1.4	1.4
Taper ratio, λ_V	0.6	0.6	0.6	0.6	0.6	0.6
Quarter-chord sweep angle, Λ, deg	0	45	0	0	45	45
NACA airfoil section	65A008	65A008	65A008	65A008	65A008	65A008
Area, S_V, sq in.	48.6	48.6	65.95	38.01	70.01	37.96
Span, b_V, in.	9.9	8.25	11.3	8.71	9.9	7.3
Mean aerodynamic chord, $\bar{c}_V$, in.	5.02	6.02	5.87	4.46	7.23	5.32
Tail length, l_V, in.	16.7	16.7	16.7	16.7	16.7	16.7
Distance from root chord to $\bar{c}_V/4$, h, in.	4.54	3.78	5.28	4	4.55	3.35

	H_1	H_2
Horizontal tail:		
Aspect ratio, A_H	4	2.77
Taper ratio, λ_H	0.6	0.6
Quarter-chord sweep angle, Λ, deg	0	45
NACA airfoil section	65A008	65A008
Area, S_H, sq in.	64.8	64.8
Span, b_H, in.	16.1	13.4
Mean aerodynamic chord, $\bar{c}_H$, in.	4.11	4.94
Tail length, l_H, in.	16.7	16.7

	F_1	F_2	F_3	F_4
Fuselage:				
Length, in.	45	45	45	45
Volume, cu in.	823	823	823	823
Side area, sq in.	206	186	250	136

TABLE III.- CONFIGURATIONS INVESTIGATED

Configuration	Basic data							Figure
Complete models (with original tails)	C_L	C_D	C_m	C_{Y_β}	C_{l_β}	C_{n_β}	plotted against α	6 11
	C_Y	C_l	C_n				plotted against β	14 to 17
Complete models (with modified tails)	C_{Y_β}	C_{l_β}	C_{n_β}				plotted against α	13
Wing-fuselage	C_L	C_D	C_m	C_{Y_β}	C_{l_β}	C_{n_β}	plotted against α	7 18
Fuselage	C_L	C_D	C_m	C_{Y_β}	C_{l_β}	C_{n_β}	plotted against α	8 19
Fuselage-tail (with original tails)	C_L	C_D	C_m	C_{Y_β}	C_{l_β}	C_{n_β}	plotted against α	9 20
Wing, isolated tail, and wing-tail (with original tails)	C_L	C_D	C_m	C_{Y_β}	C_{l_β}	C_{n_β}	plotted against α	10 22

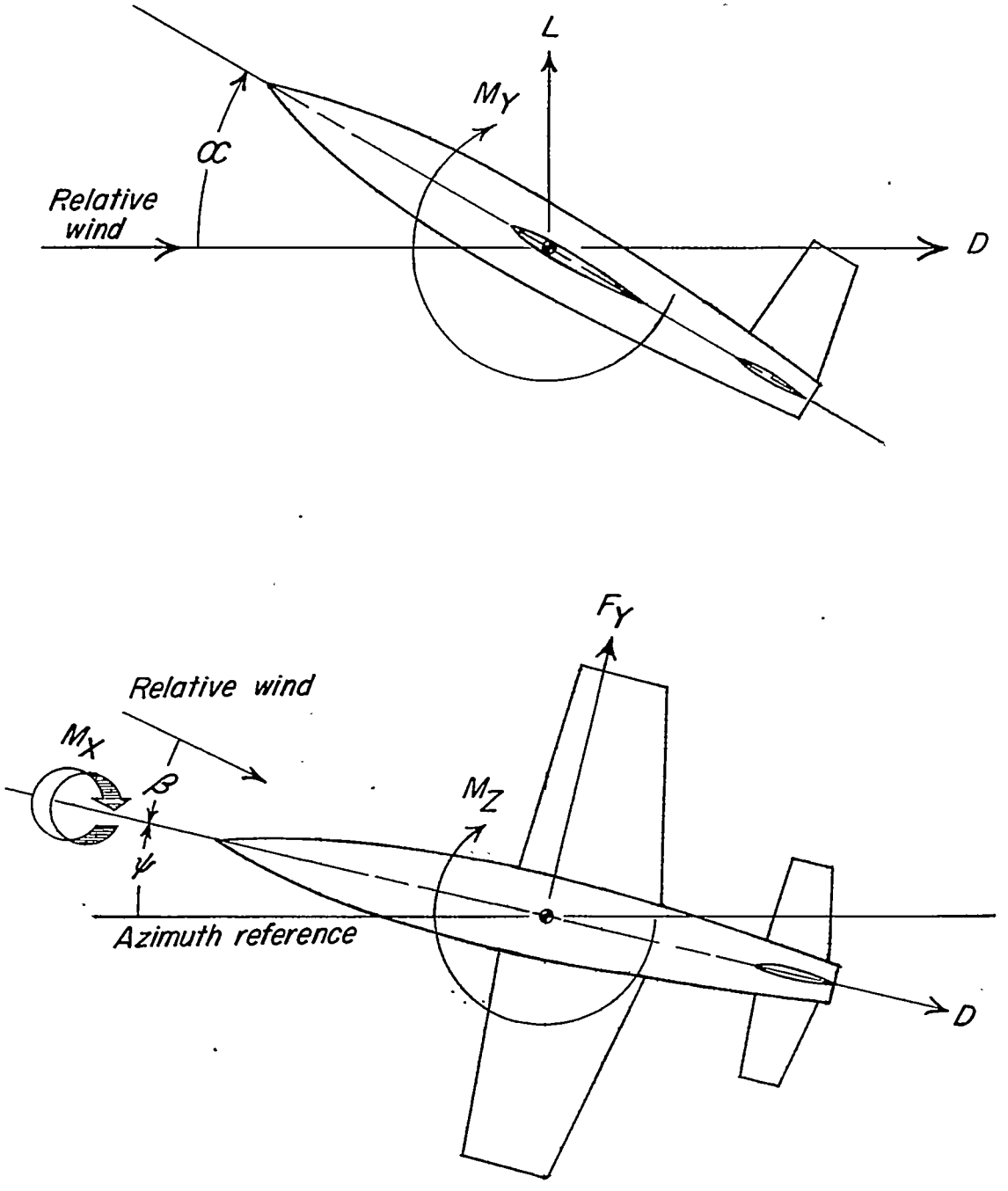

Figure 1.- Stability system of axes. Arrows indicate positive direction of angles, forces, and moments.

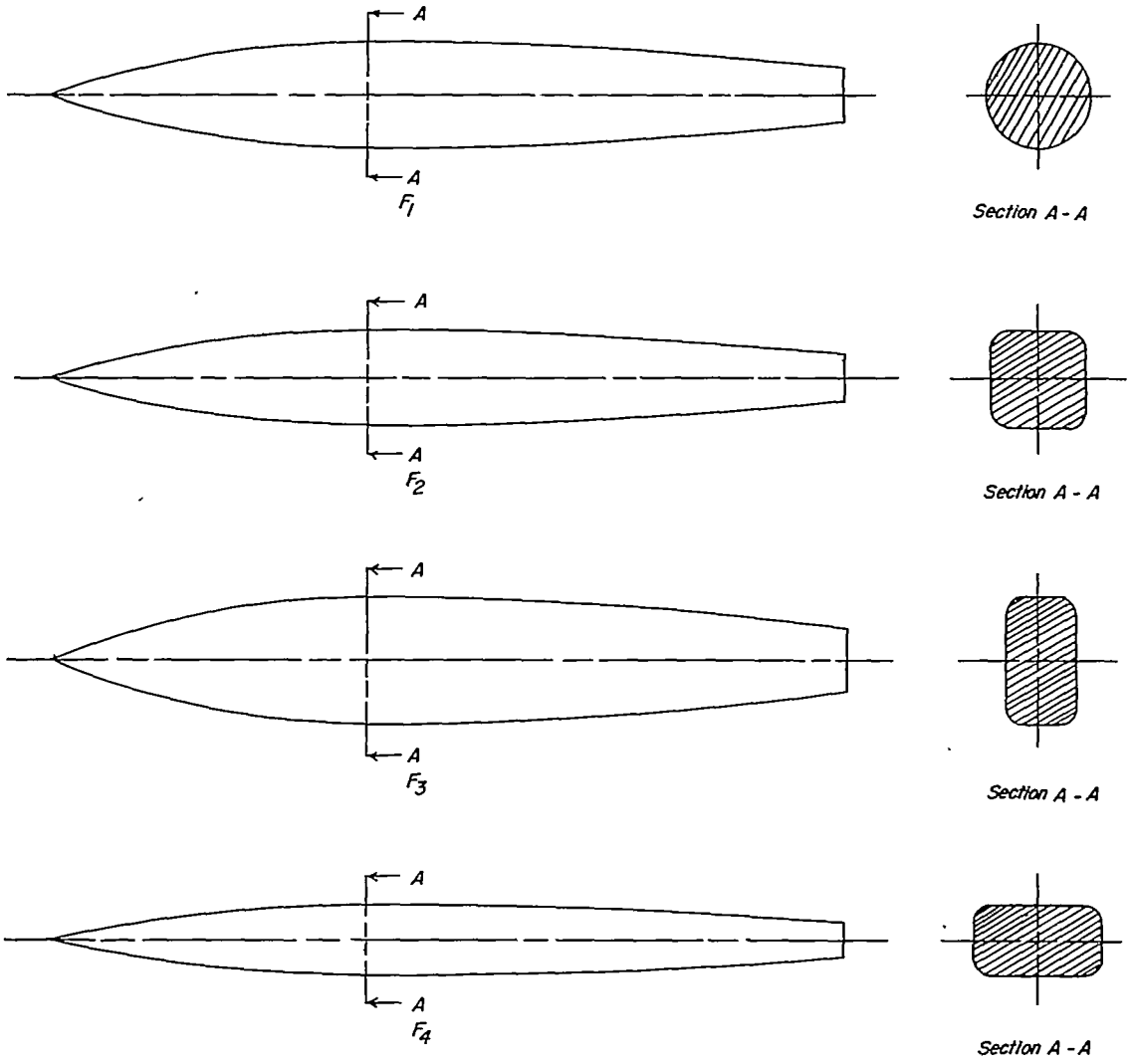

Figure 2.- Side views of fuselages.

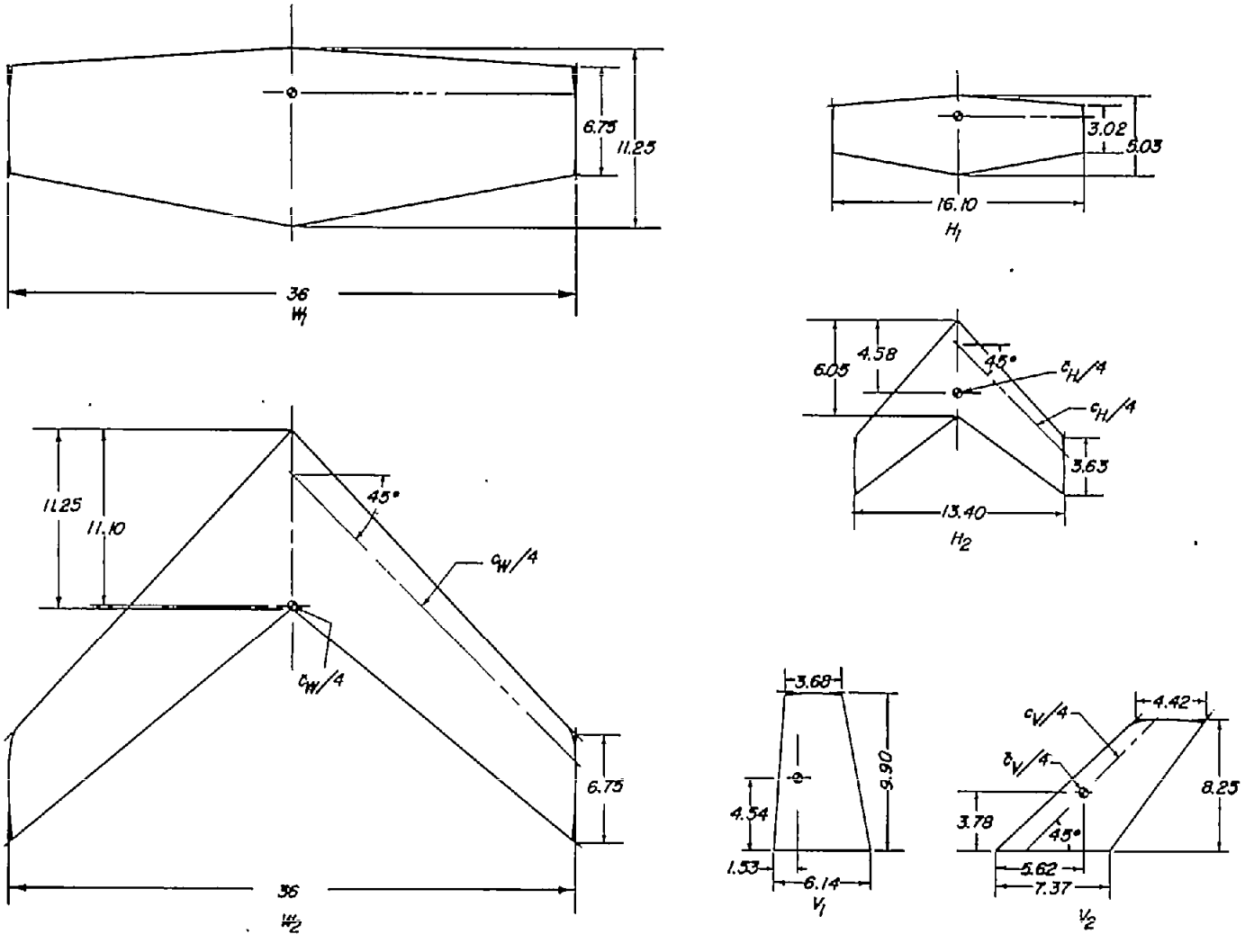

Figure 3.- Geometric characteristics of the wings and of the original horizontal and vertical tails. All dimensions are in inches.

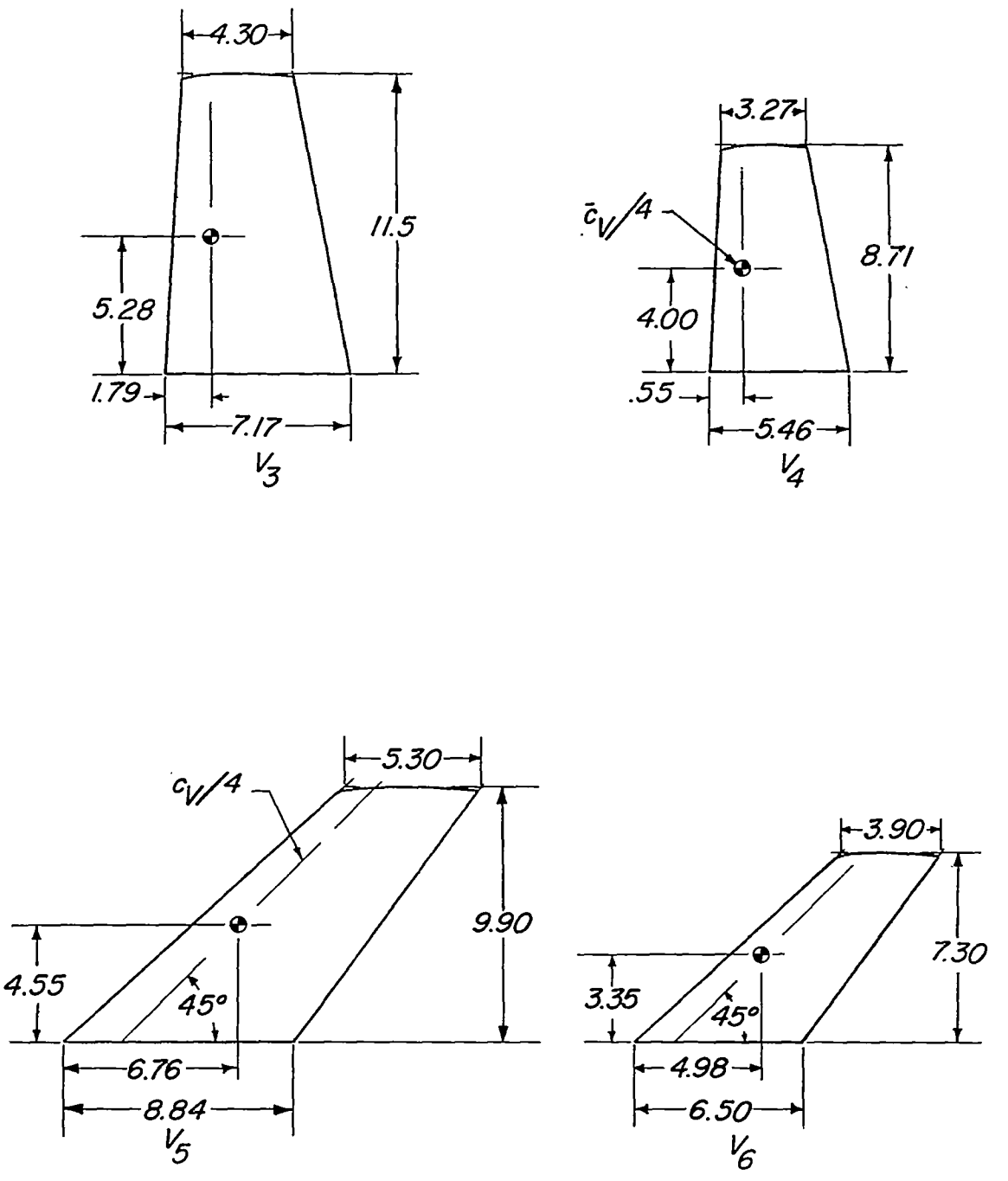

Figure 4.- Geometric characteristics of the modified vertical tails. All dimensions are in inches.

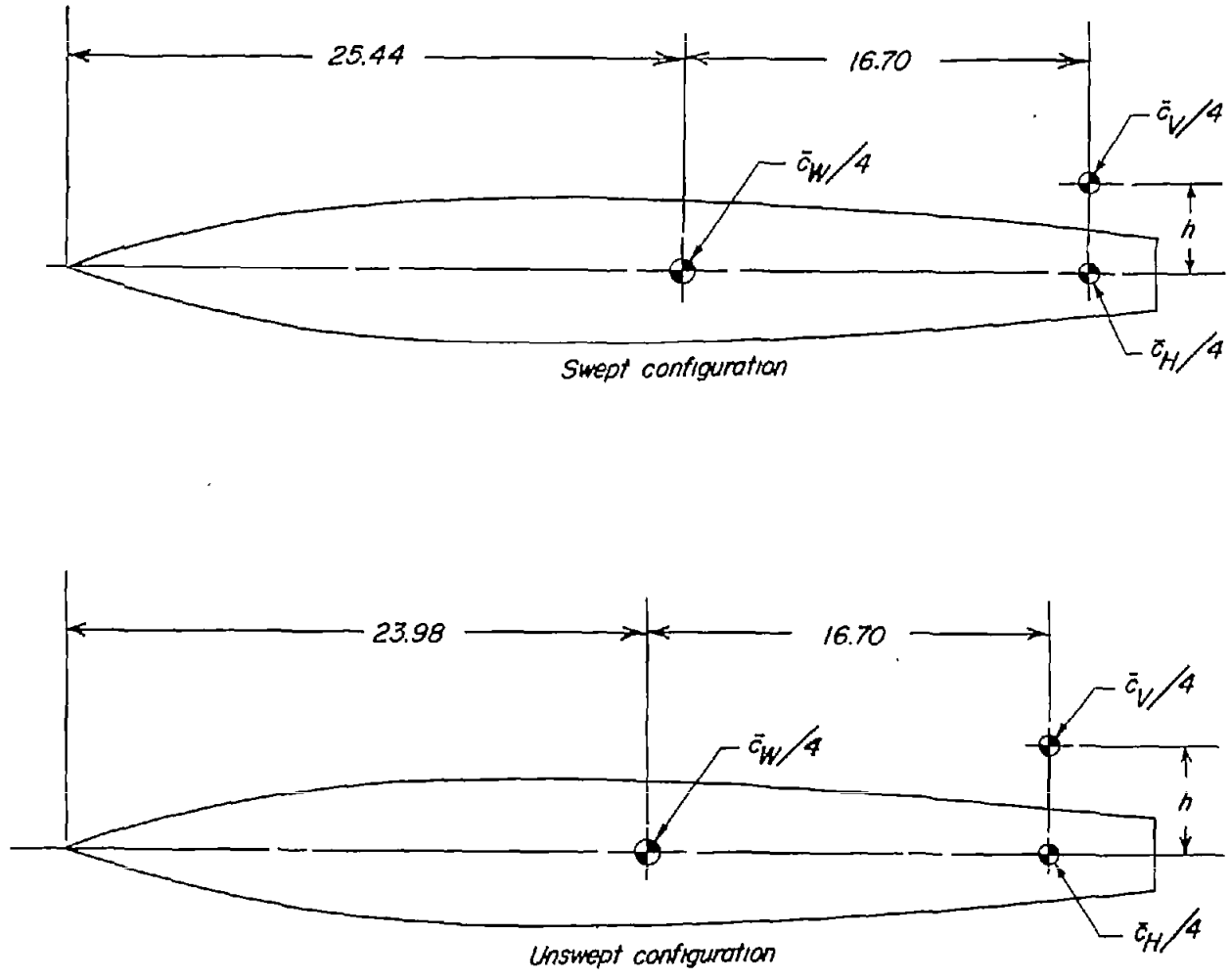

Figure 5.- Sketch of circular-cross-section fuselage with dimensions which give relative positions of the wing, tails, and fuselage. All dimensions are in inches.

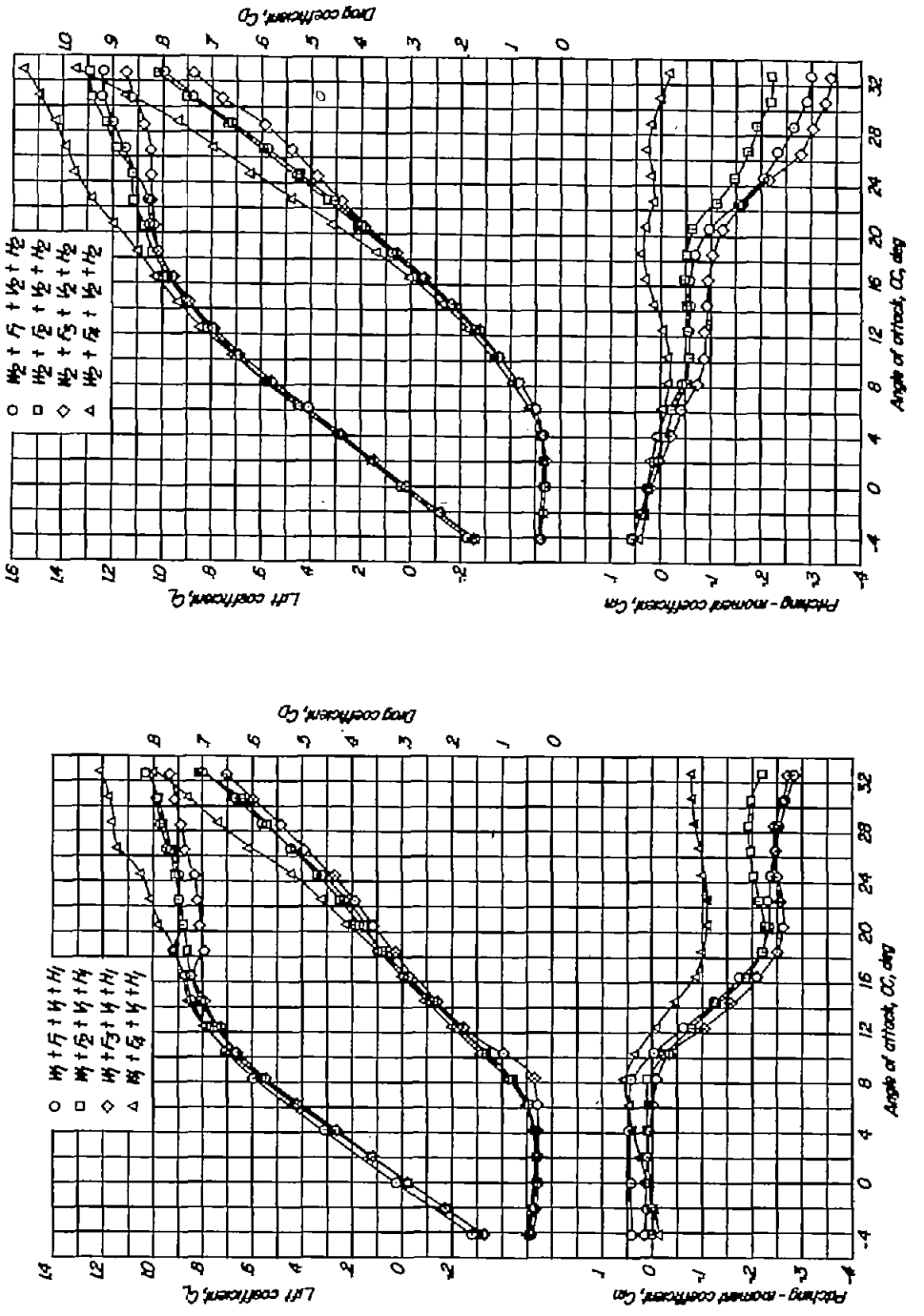

(a) $\Lambda = 0^\circ$.

(b) $\Lambda = 45^\circ$.

Figure 6.- Effect of fuselage cross section on the static longitudinal stability characteristics of several unswept and 45° sweptback wing-fuselage-tail configurations.

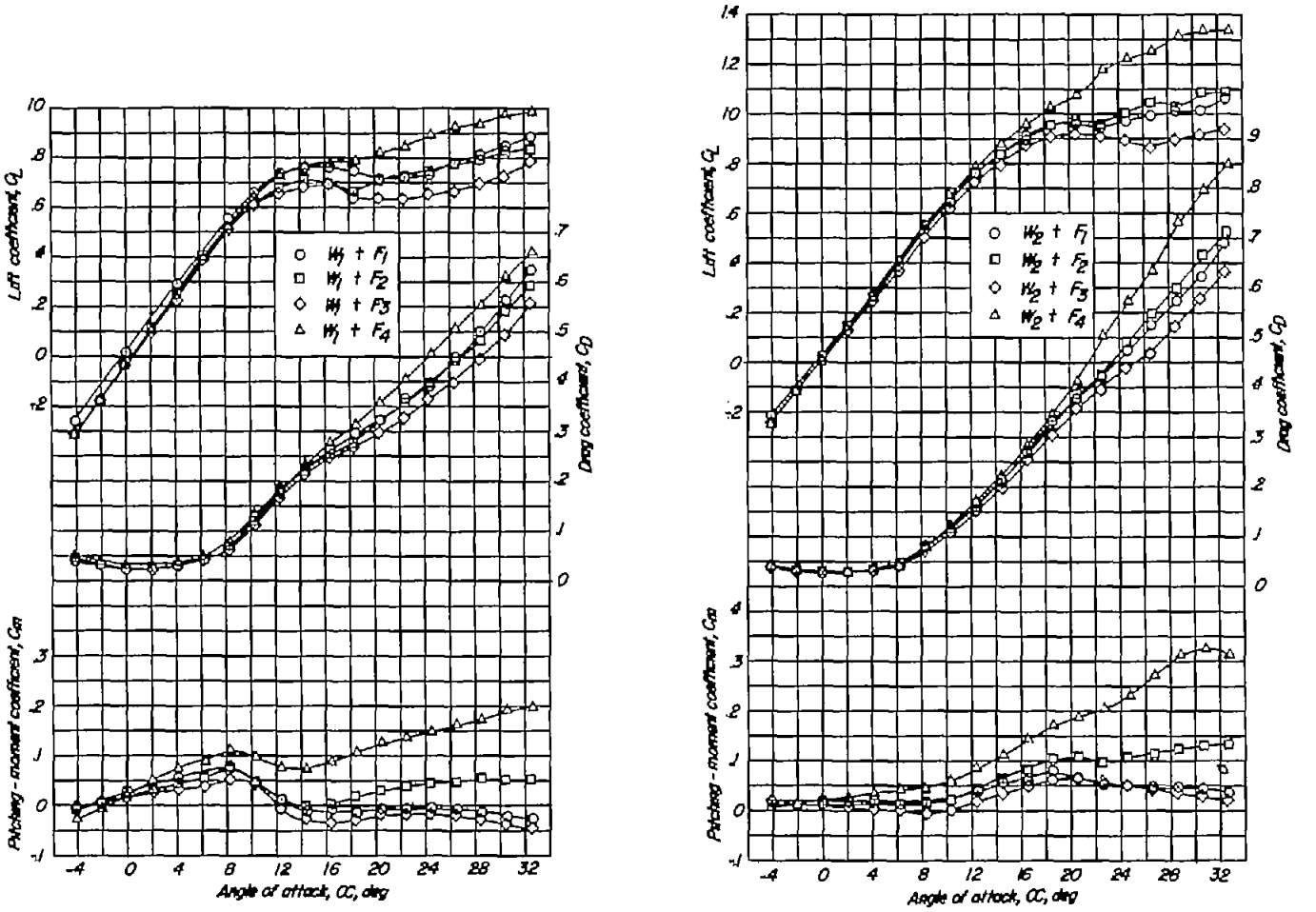

(a) $\Lambda = 0°$.

(b) $\Lambda = 45°$.

Figure 7.- Effect of fuselage cross section on the static longitudinal stability characteristics of several unswept and 45° sweptback wing-fuselage configurations.

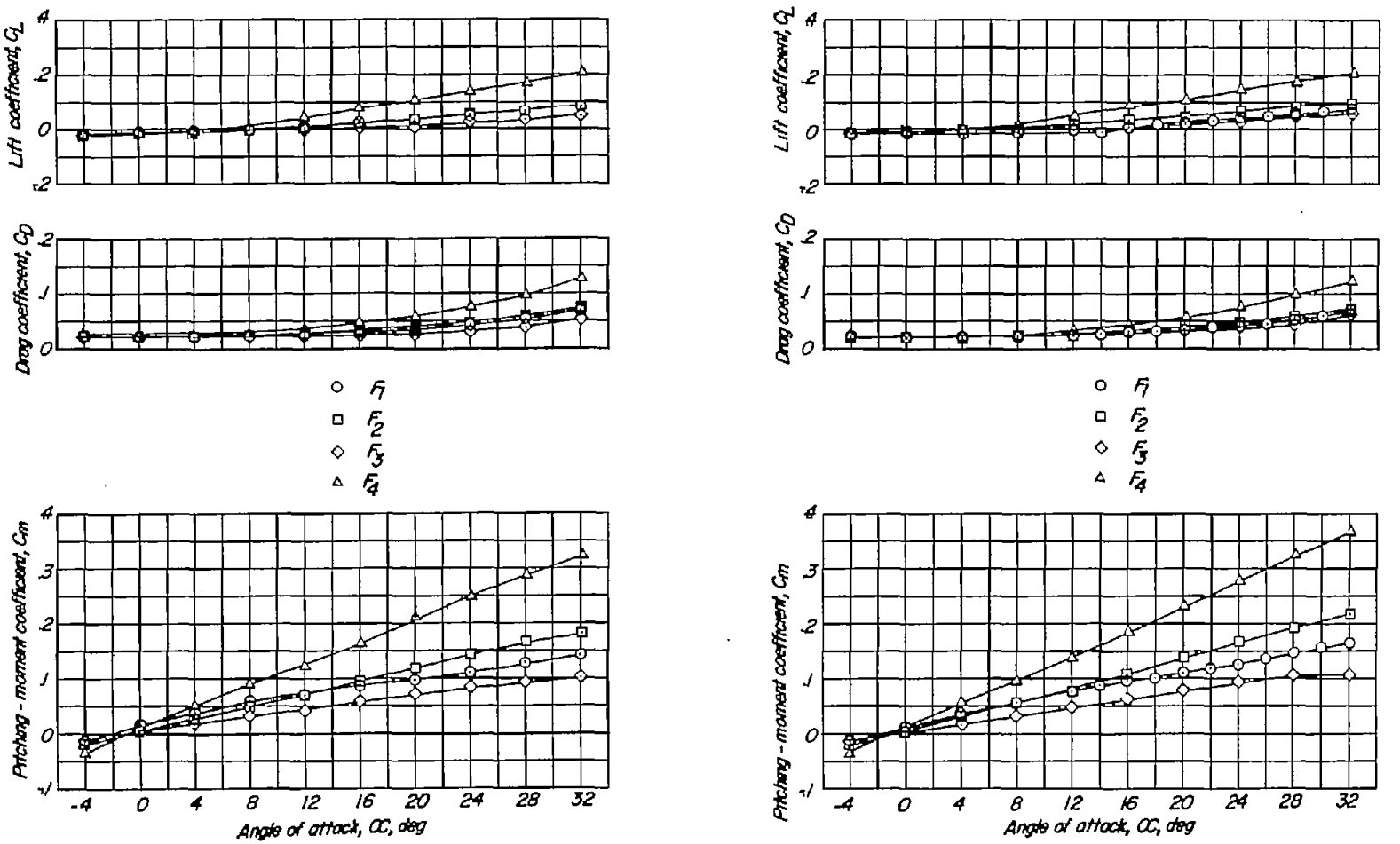

(a) Center of gravity for $\Lambda = 0°$. (b) Center of gravity for $\Lambda = 45°$.

Figure 8.- Effect of fuselage cross section on the static longitudinal stability characteristics of several fuselage configurations with different center-of-gravity locations.

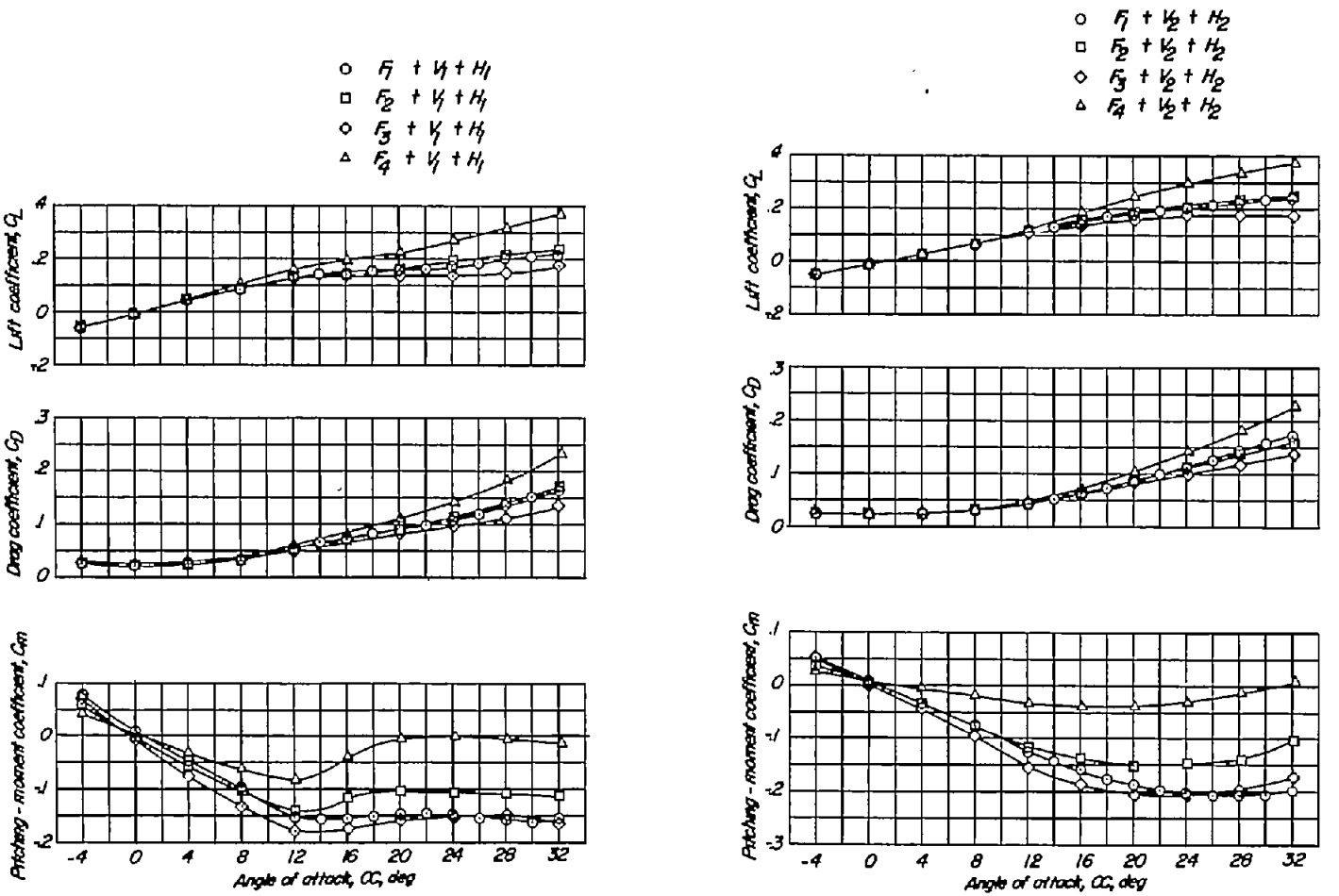

(a) $\Lambda = 0^\circ$.

(b) $\Lambda = 45^\circ$.

Figure 9.- Effect of fuselage cross section on the static longitudinal stability characteristics of several fuselages in combination with unswept and 45° sweptback tail configurations.

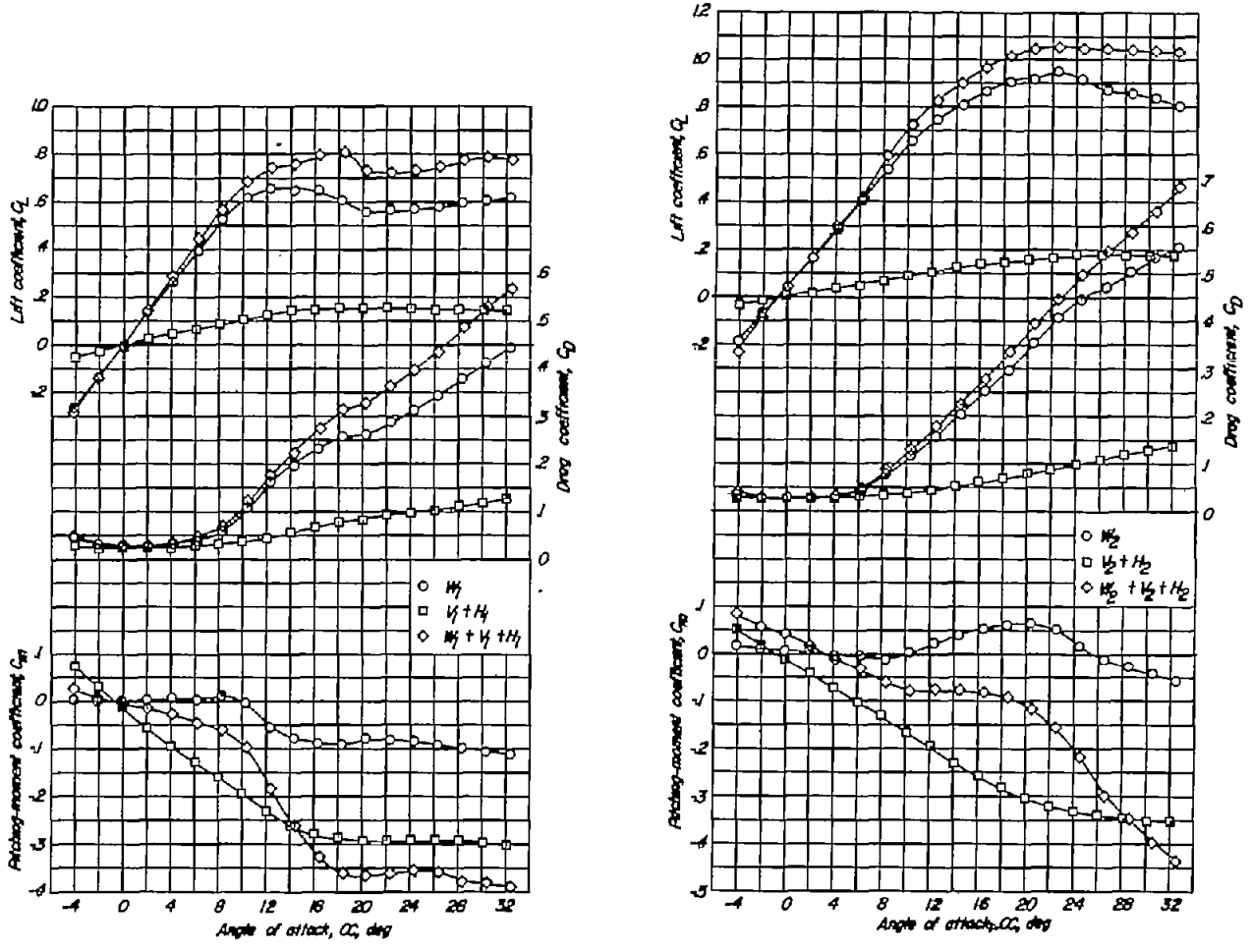

(a) $\Lambda = 0^\circ$.

(b) $\Lambda = 45^\circ$.

Figure 10.- Comparison of the static longitudinal stability characteristics of unswept and 45° sweptback wings, unswept and 45° sweptback isolated tails, and unswept and 45° sweptback wings in combination with unswept and 45° sweptback tails.

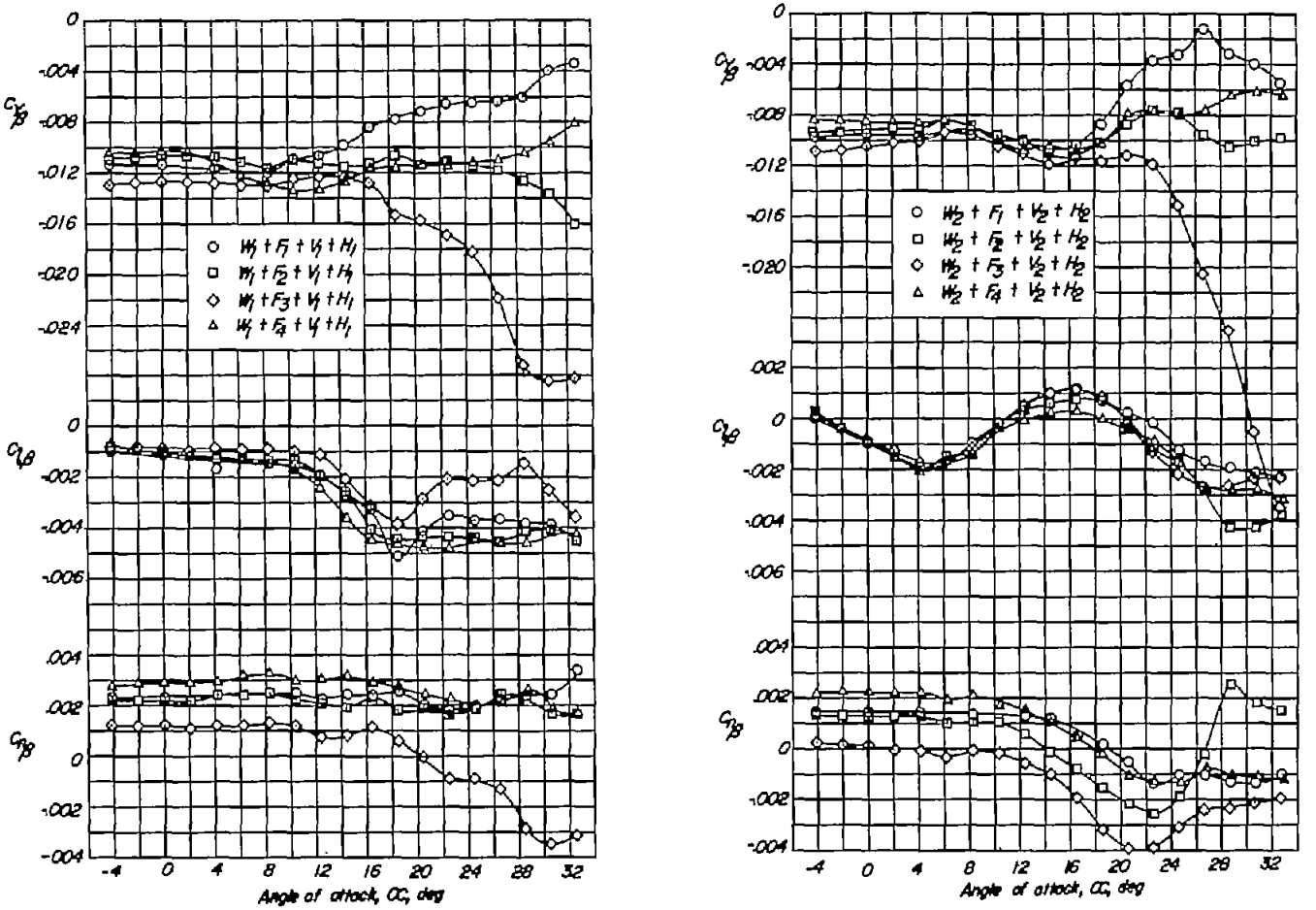

(a) $\Lambda = 0^\circ$.

(b) $\Lambda = 45^\circ$.

Figure 11.- Effect of fuselage cross section on the static lateral stability characteristics of several unswept and 45° sweptback wing-fuselage-tail configurations.

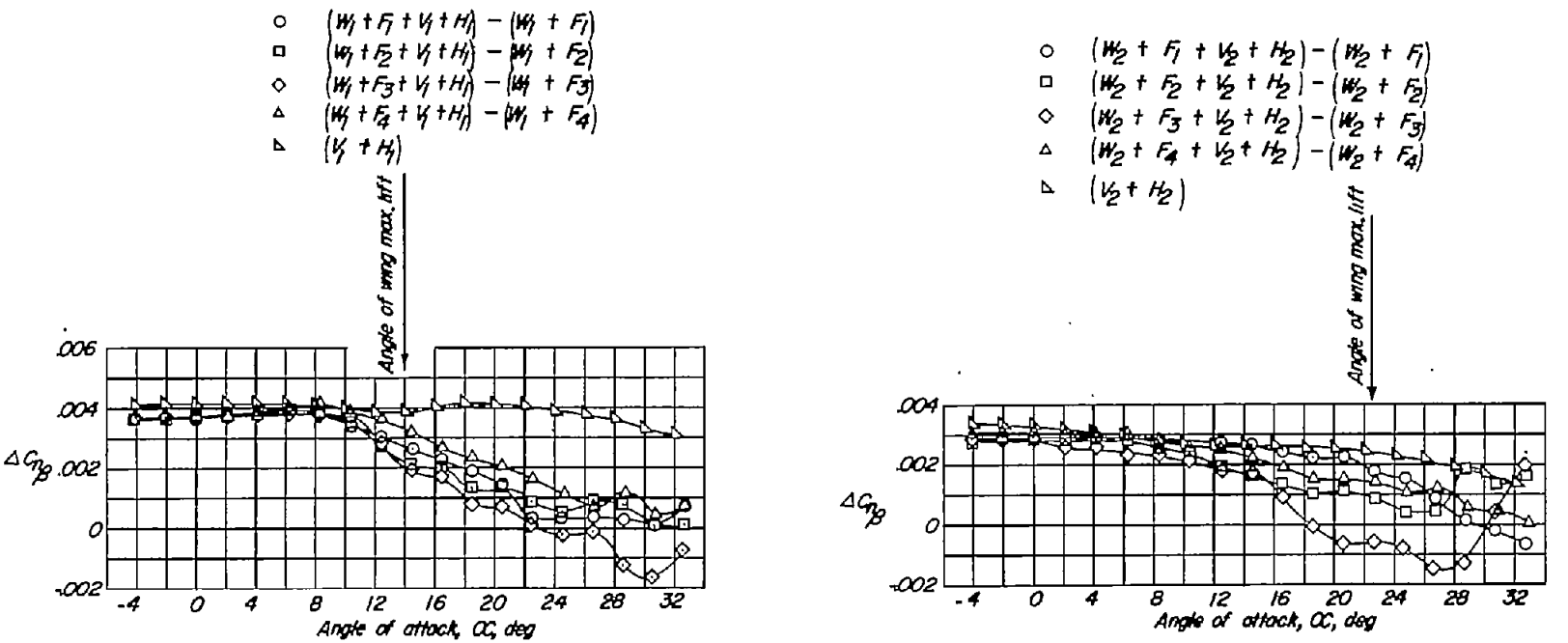

(a) $\Lambda = 0^\circ$.

(b) $\Lambda = 45^\circ$.

Figure 12.- Effect of fuselage cross section on the tail contribution to C_{n_β} for the unswept and 45° sweptback complete-model configurations.

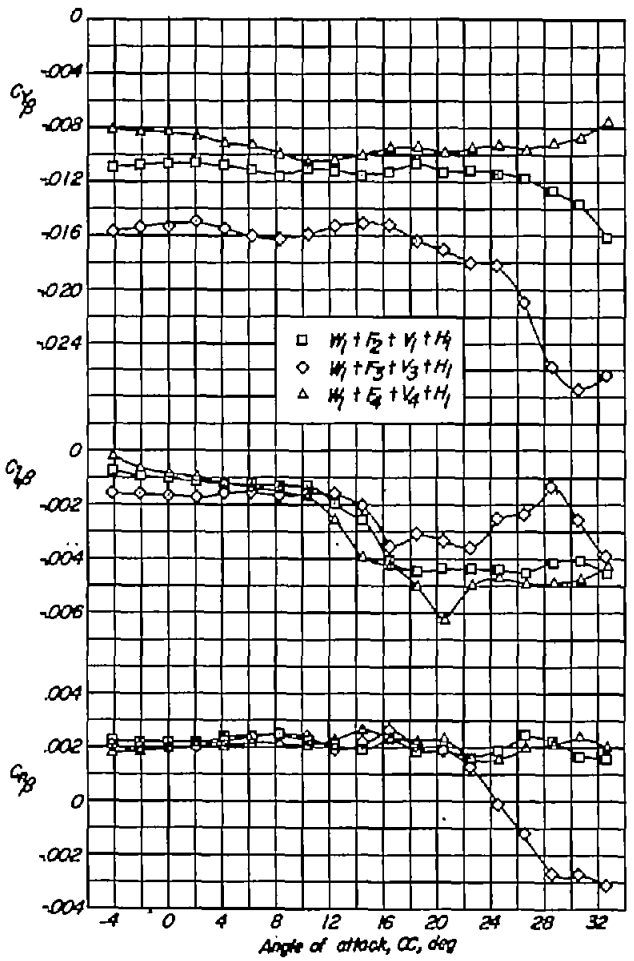

(a) $\Lambda = 0^\circ$.

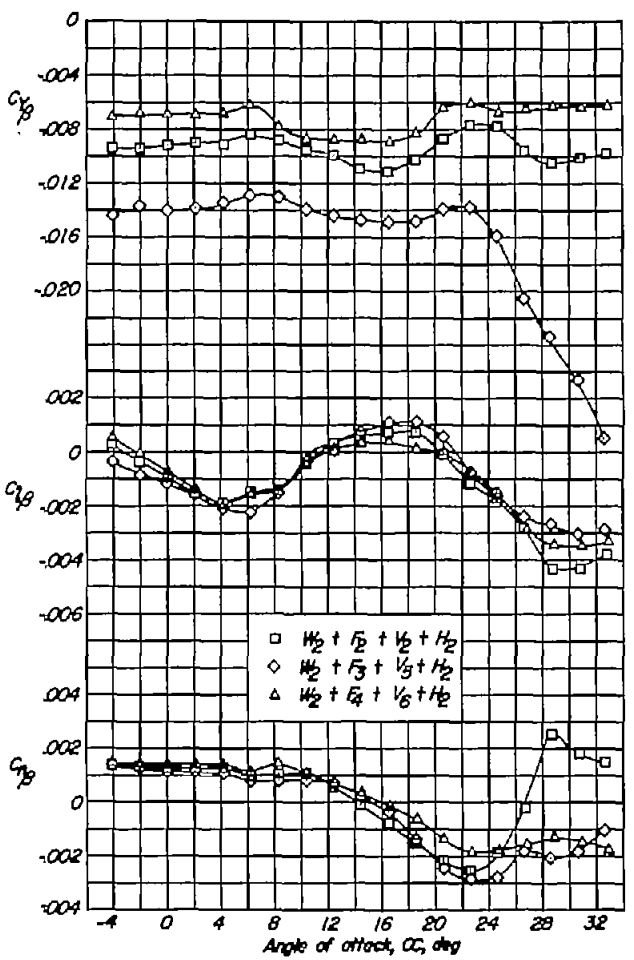

(b) $\Lambda = 45^\circ$.

Figure 13.- Effect of fuselage cross section on the static lateral stability characteristics of several unswept and 45° sweptback wing-fuselage-tail configurations. Modified tails.

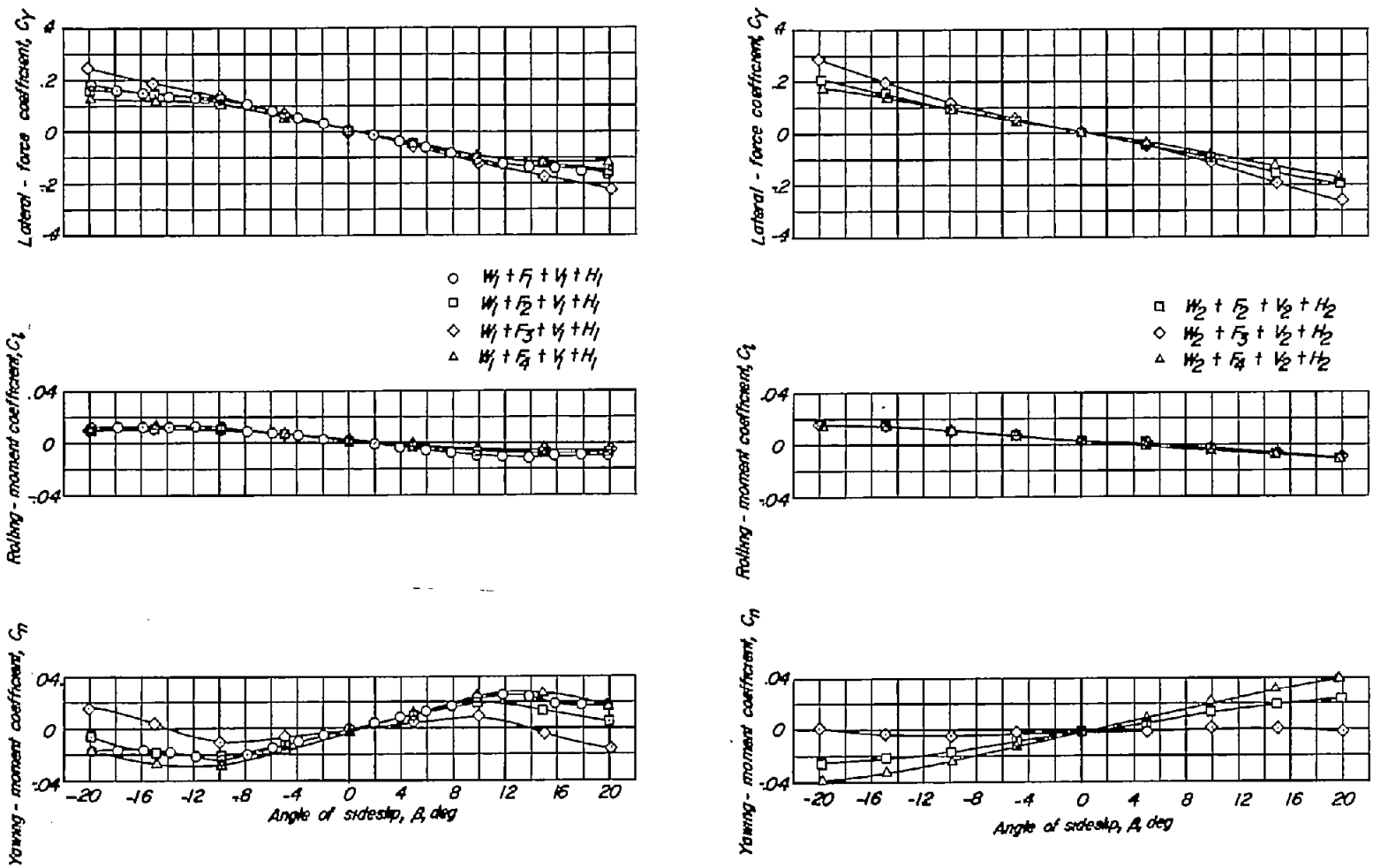

(a) $\Lambda = 0^\circ$.

(b) $\Lambda = 45^\circ$.

Figure 14.- Effect of fuselage cross section on the static lateral stability characteristics of an unswept and 45° sweptback wing-fuselage-tail configuration through the sideslip range. $\alpha = 0^\circ$.

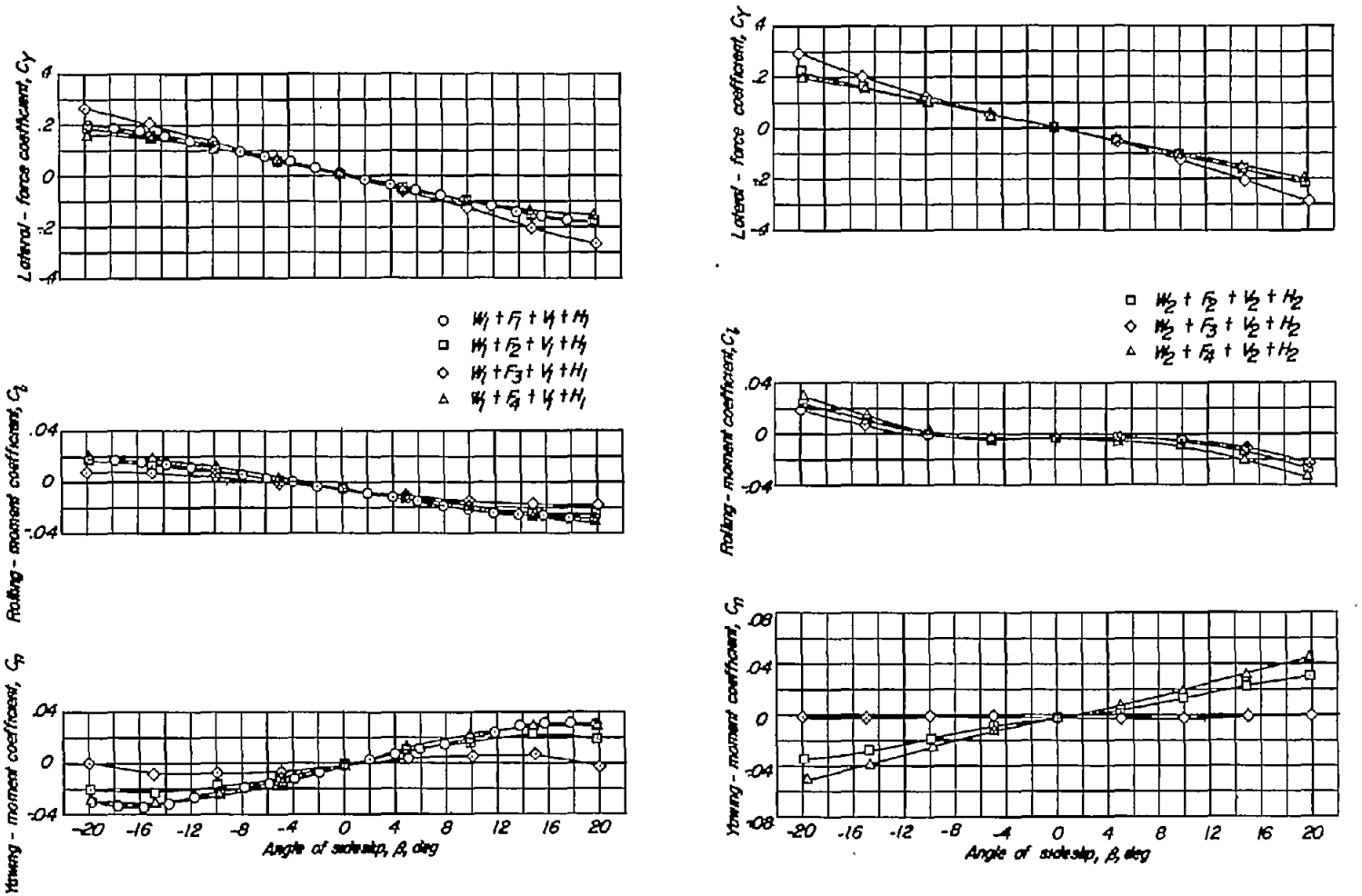

(a) $\Lambda = 0^\circ$.

(b) $\Lambda = 45^\circ$.

Figure 15.- Effect of fuselage cross section on the static lateral stability characteristics of an unswept and 45° sweptback wing-fuselage-tail configuration through the sideslip range. $\alpha = 10^\circ$.

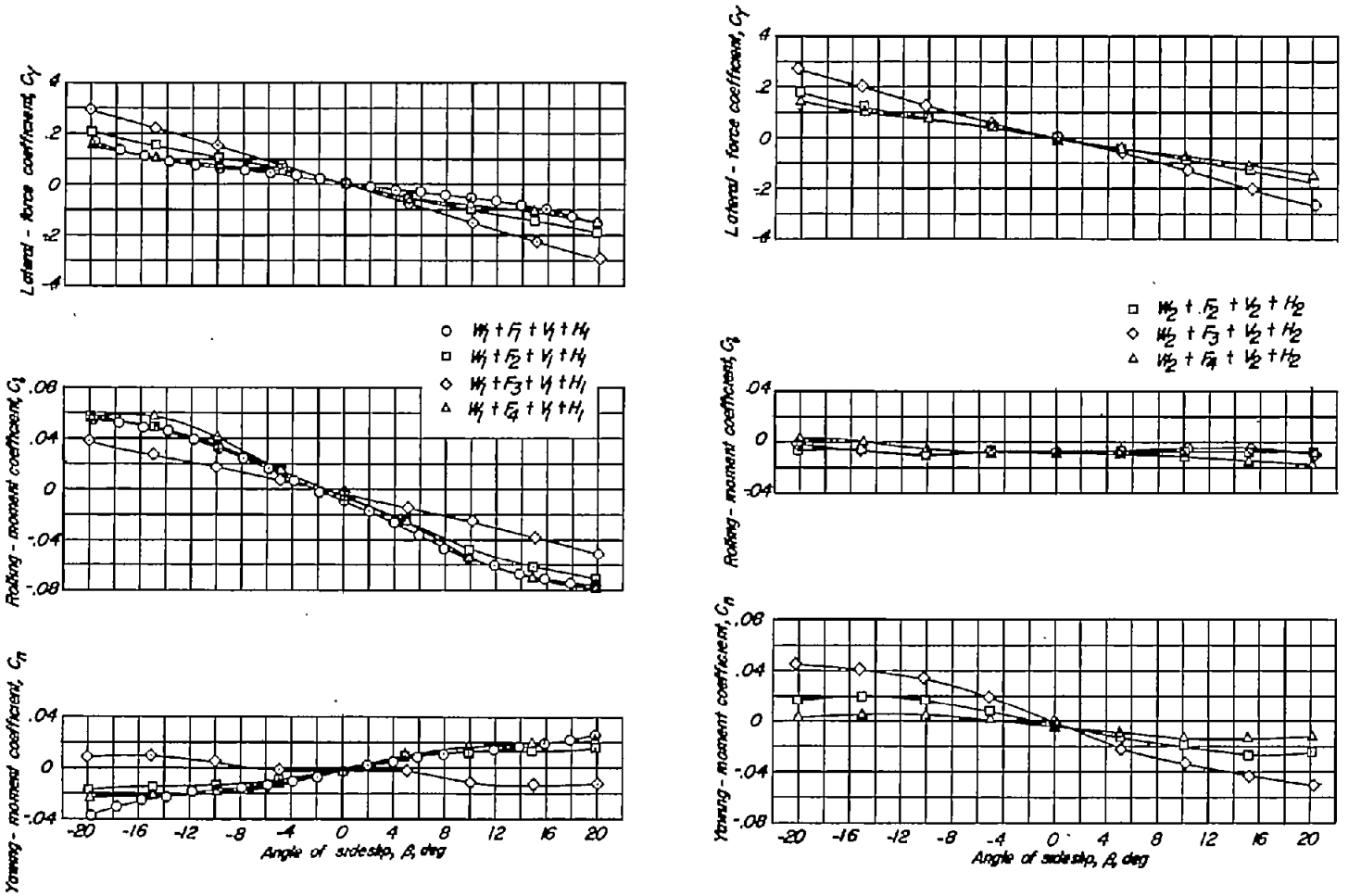

(a) $\Lambda = 0^\circ$.

(b) $\Lambda = 45^\circ$.

Figure 16.- Effect of fuselage cross section on the static lateral stability characteristics of an unswept and 45° sweptback wing-fuselage-tail configuration through the sideslip range. $\alpha = 20^\circ$.

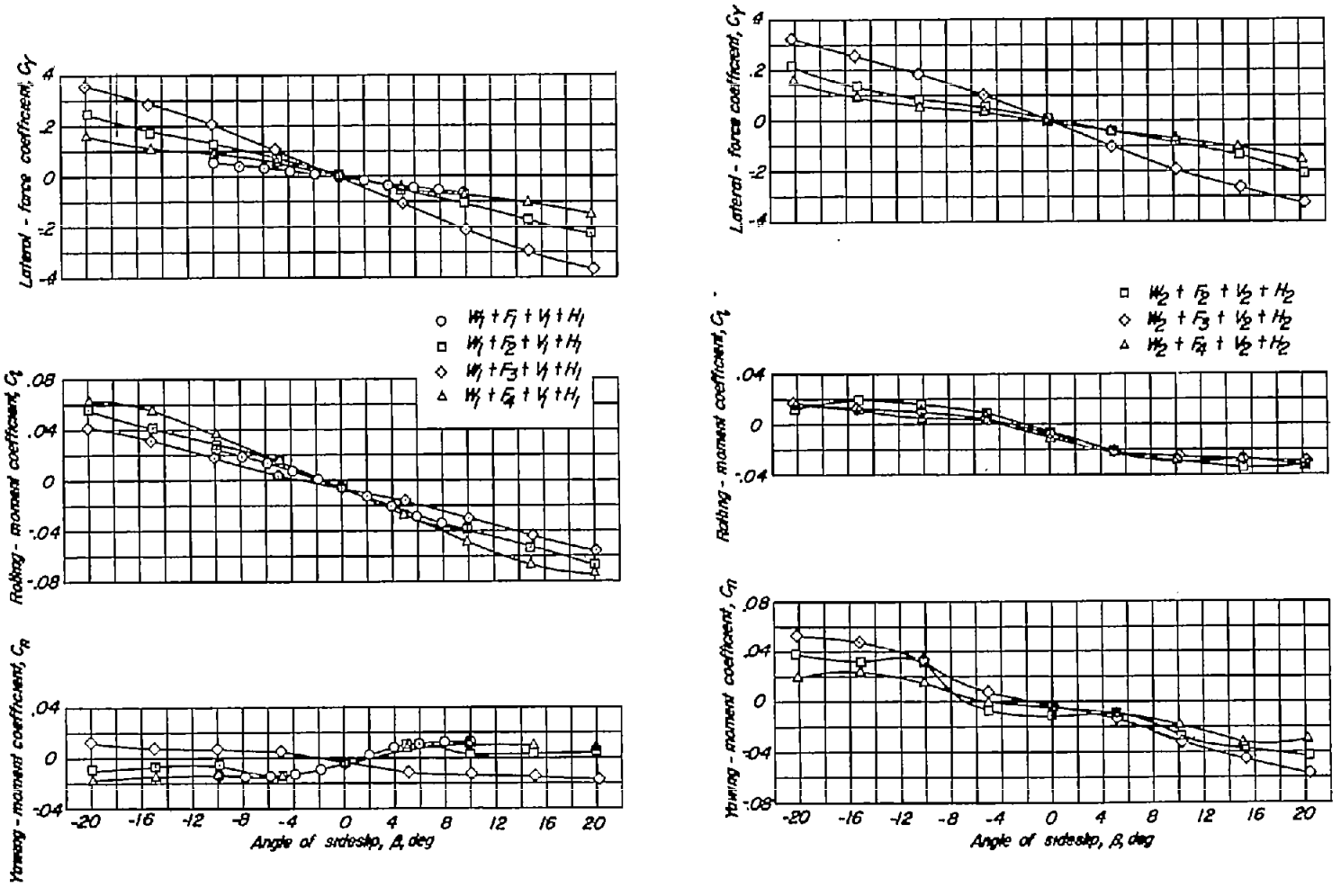

(a) $\Lambda = 0°$.

(b) $\Lambda = 45°$.

Figure 17.- Effect of fuselage cross section on the static lateral stability characteristics of an unswept and 45° sweptback wing-fuselage-tail configuration through the sideslip range. $\alpha = 26°$.

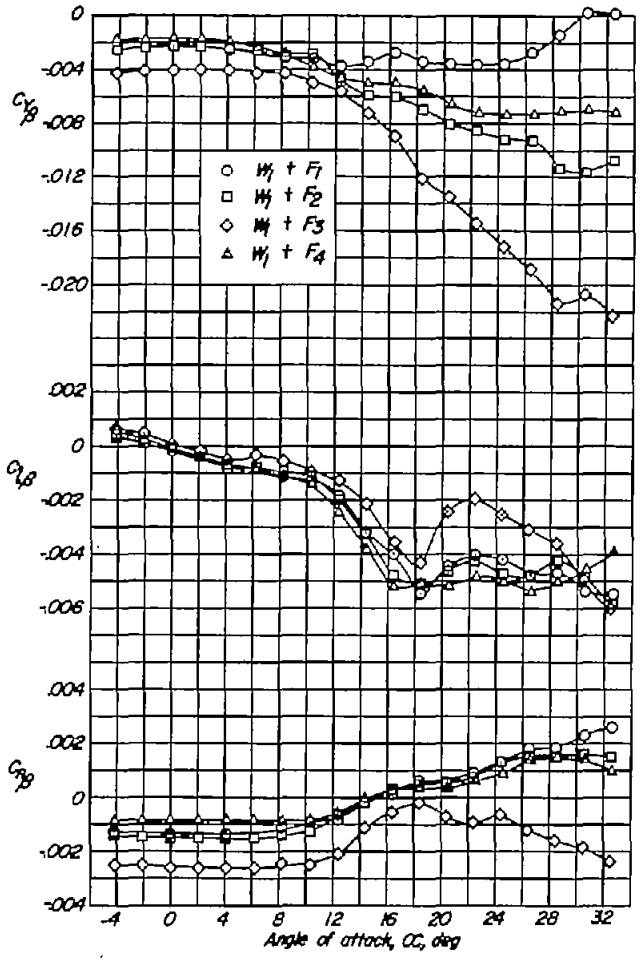

(a) $\Lambda = 0^\circ$.

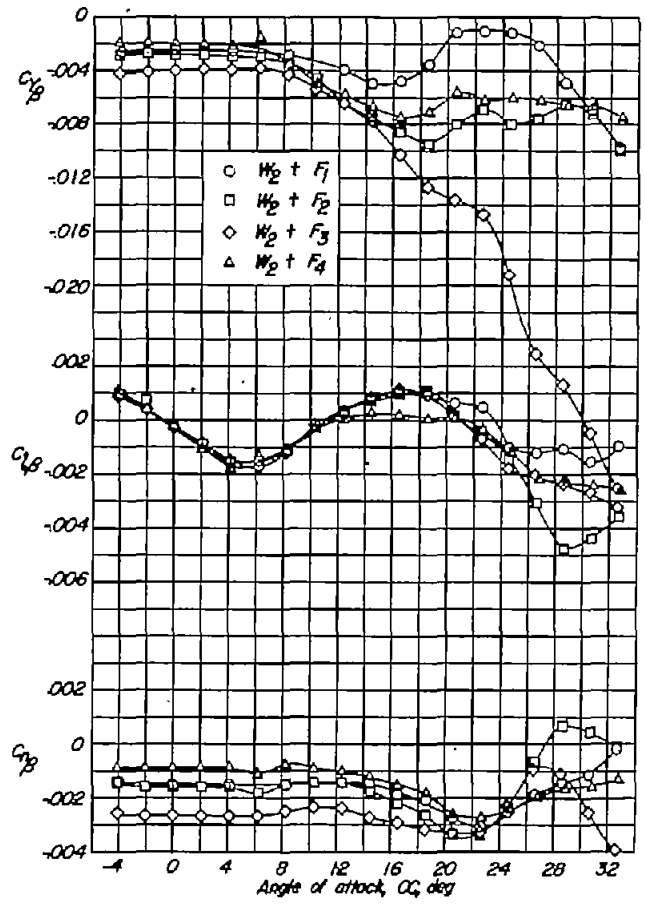

(b) $\Lambda = 45^\circ$.

Figure 18.- Effect of fuselage cross section on the static lateral stability characteristics of several unswept and 45° sweptback wing-fuselage configurations.

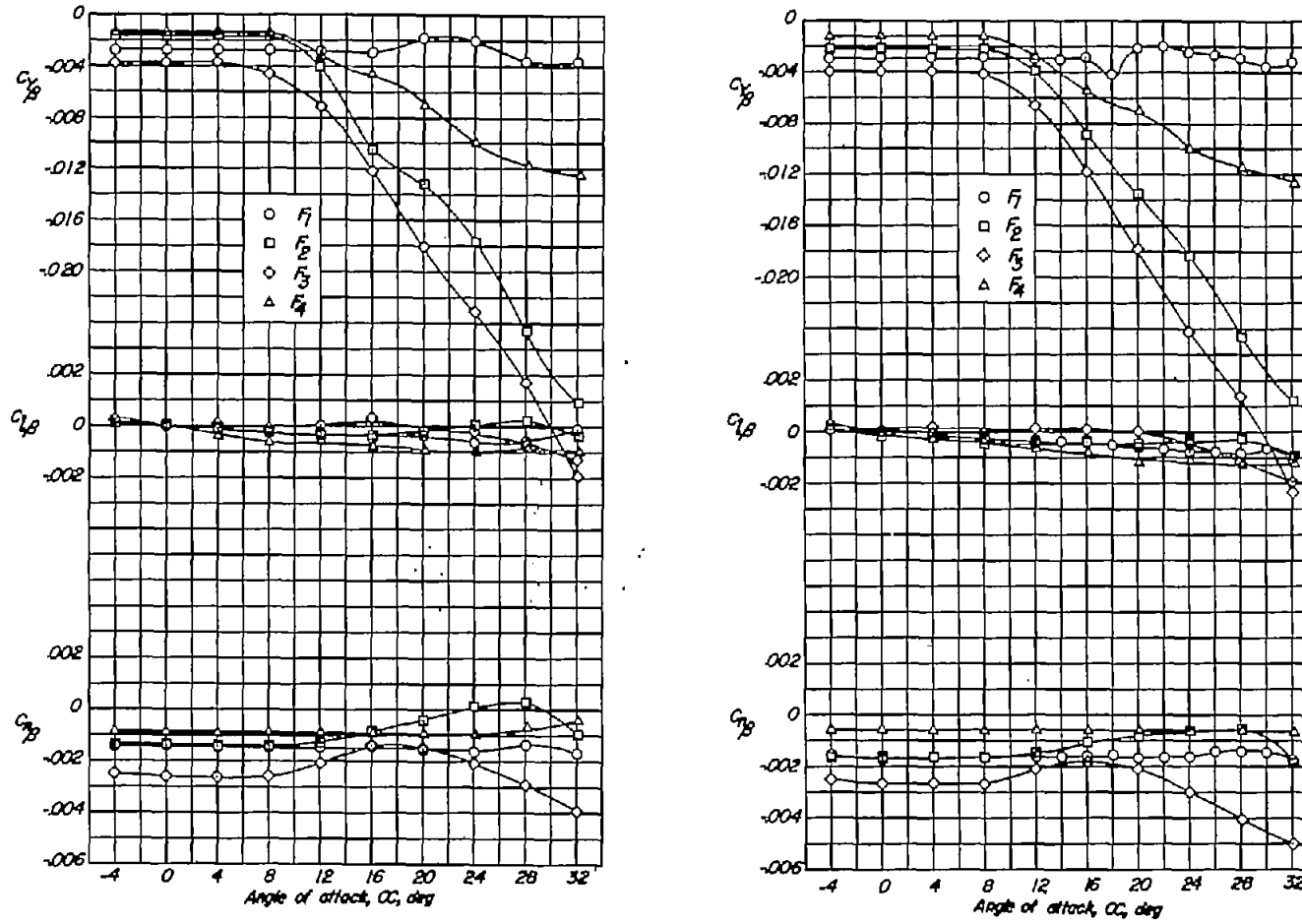

(a) Center of gravity for $\Lambda = 0^\circ$. (b) Center of gravity for $\Lambda = 45^\circ$.

Figure 19.- Effect of fuselage cross section on the static lateral stability characteristics of several fuselage configurations with different center-of-gravity locations.

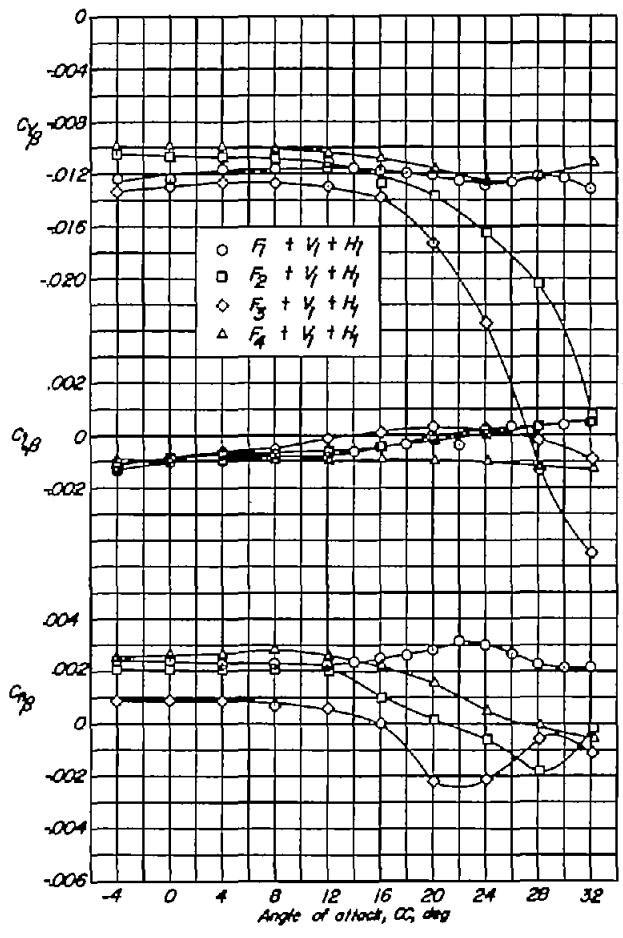

(a) $\Lambda = 0°$.

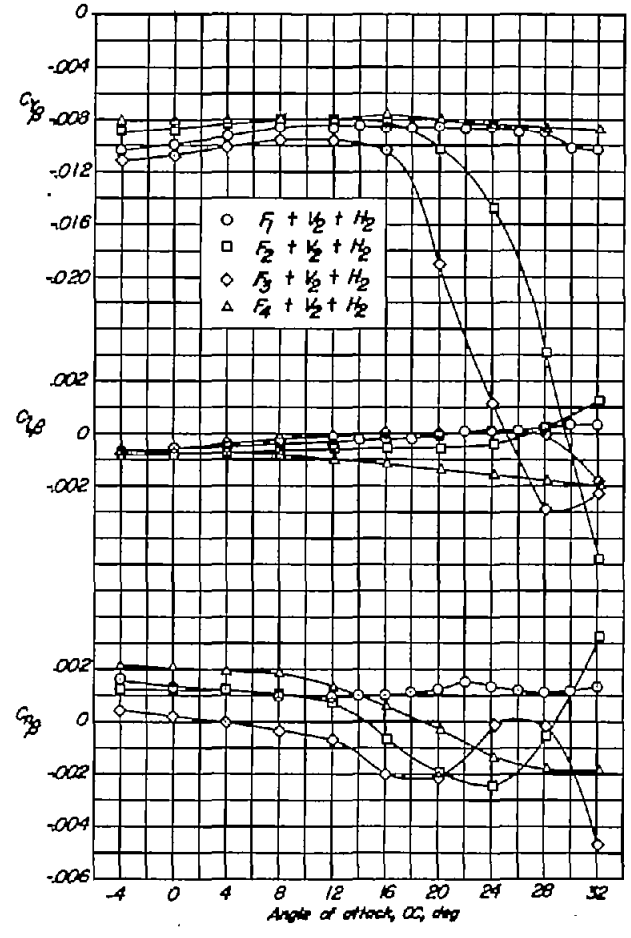

(b) $\Lambda = 45°$.

Figure 20.- Effect of fuselage cross section on the static lateral stability characteristics of several fuselages in combination with unswept and 45° sweptback tail configurations.

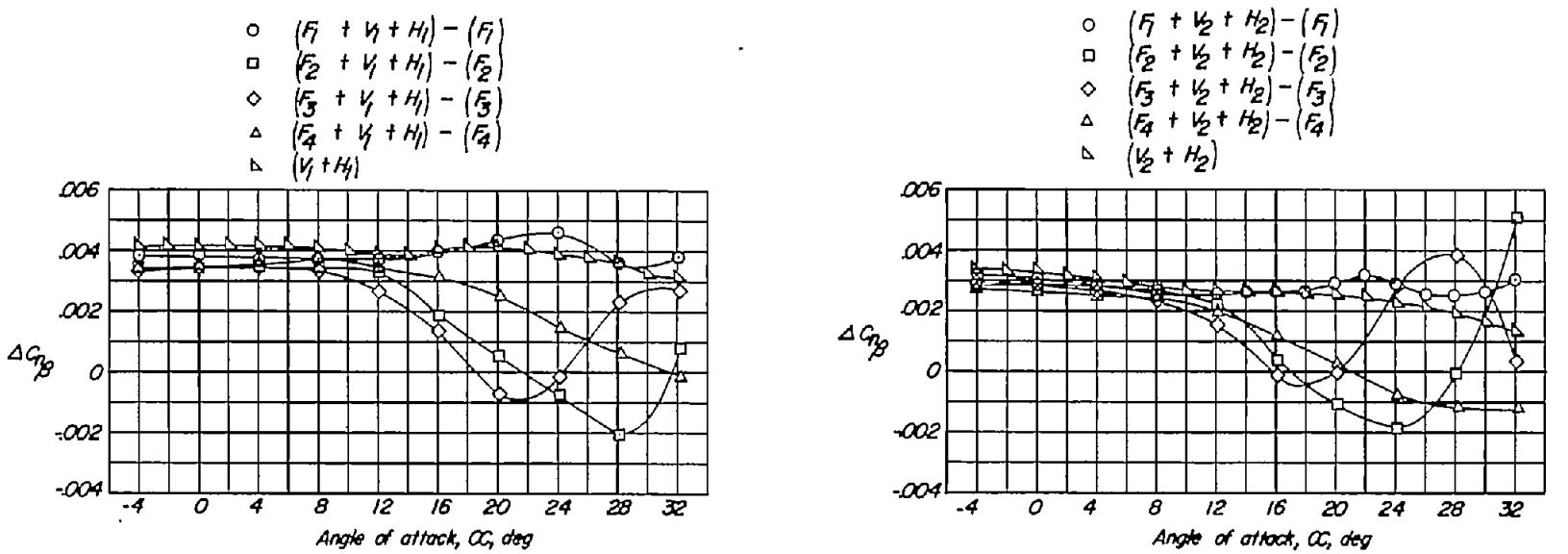

(a) $\Lambda = 0^{\circ}$.

(b) $\Lambda = 45^{\circ}$.

Figure 21.- Effect of fuselage cross section on the tail contribution to C_{n_β} for several fuselages in combination with unswept and 45° swept-back tails.

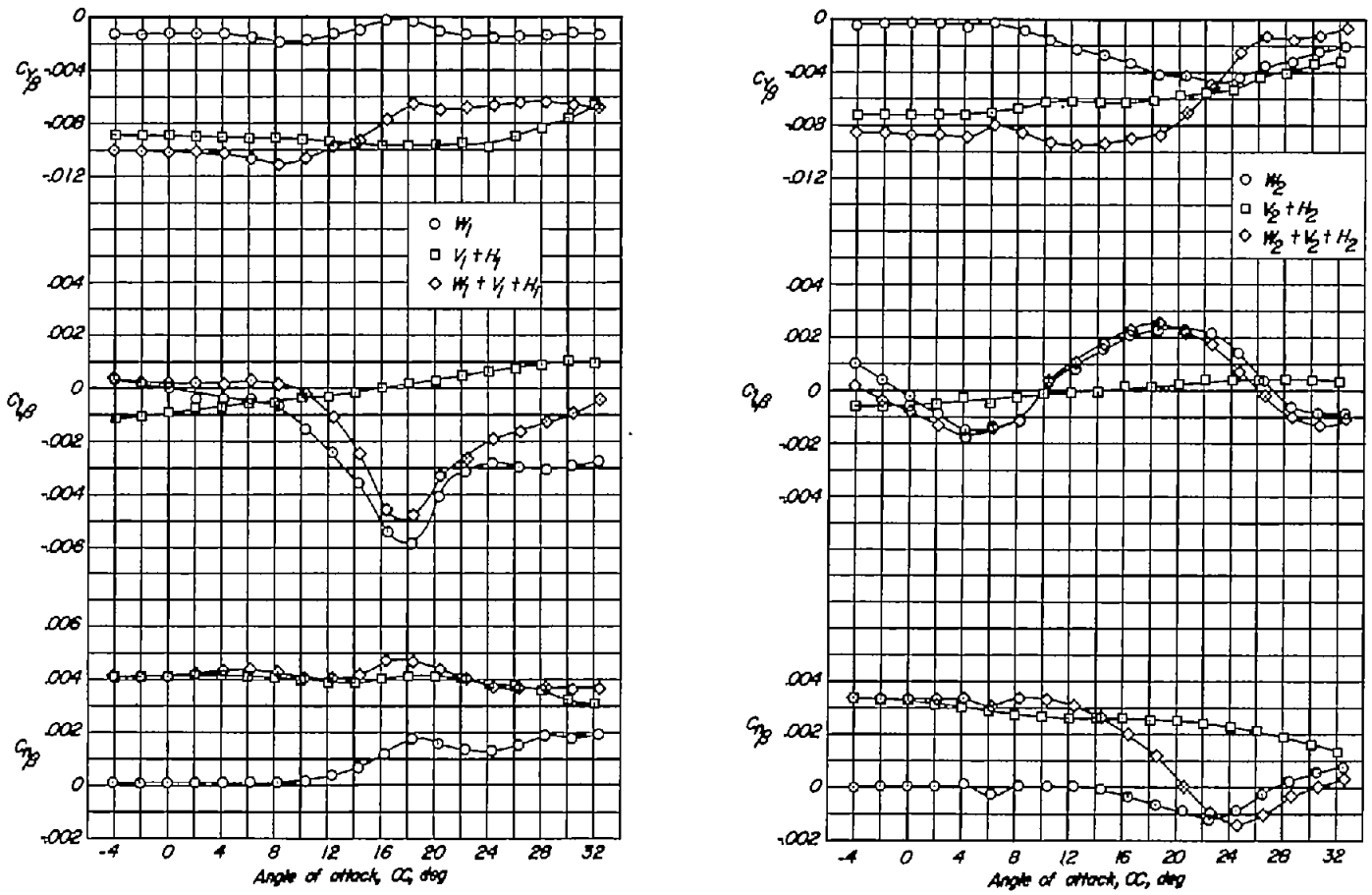

(a) $\Lambda = 0°$.

(b) $\Lambda = 45°$.

Figure 22.- Comparison of the static lateral stability characteristics of the unswept and 45° sweptback wings, unswept and 45° sweptback isolated tails, and unswept and 45° sweptback wings in combination with unswept and 45° sweptback tails.

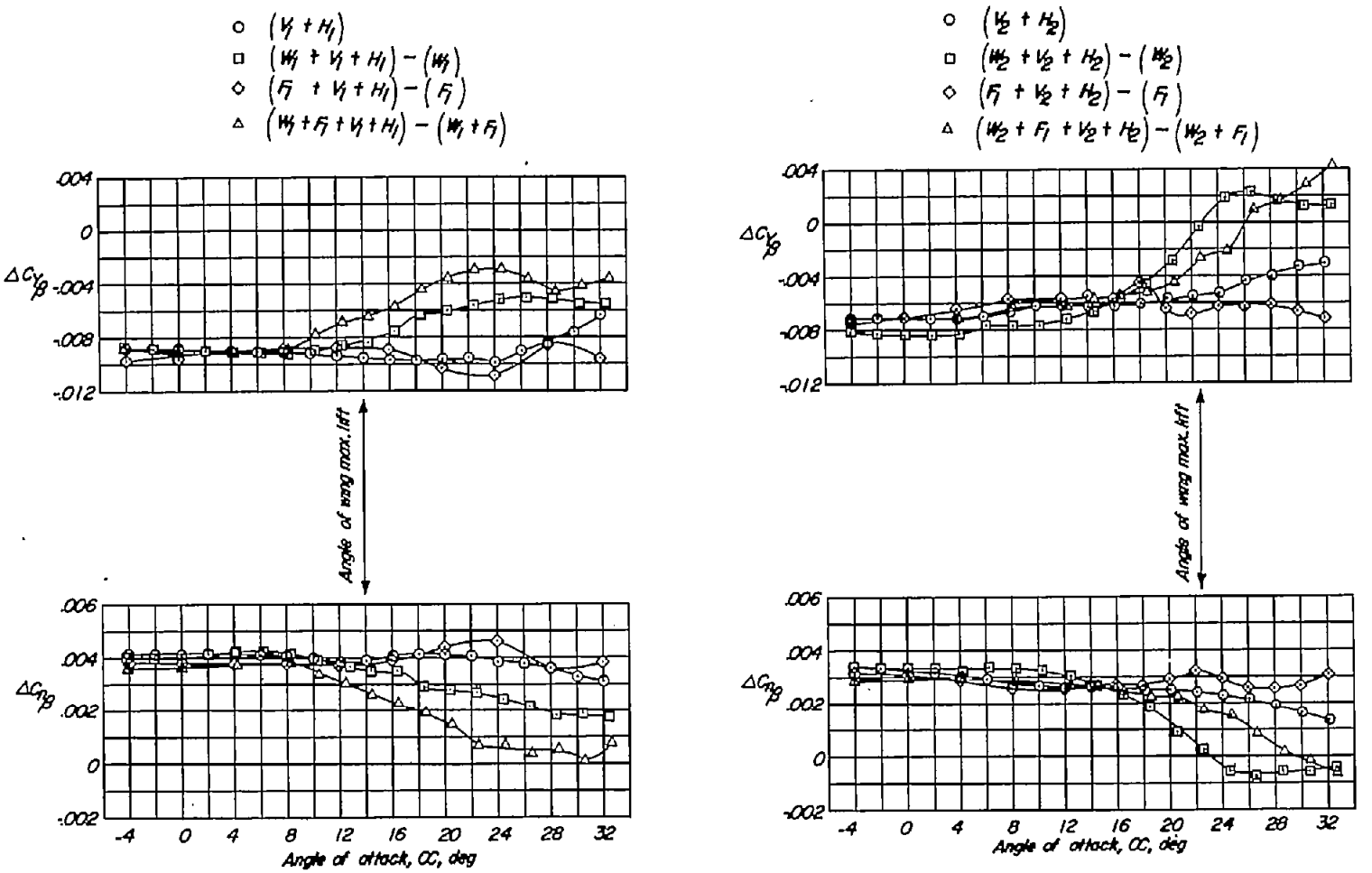

(a) $\Lambda = 0^{\circ}$.

(b) $\Lambda = 45^{\circ}$.

Figure 23.- Comparison of the effect of fuselage, wing, and wing-fuselage combination on the tail contribution to C_{Y_β} and C_{n_β}. Fuselage 1.

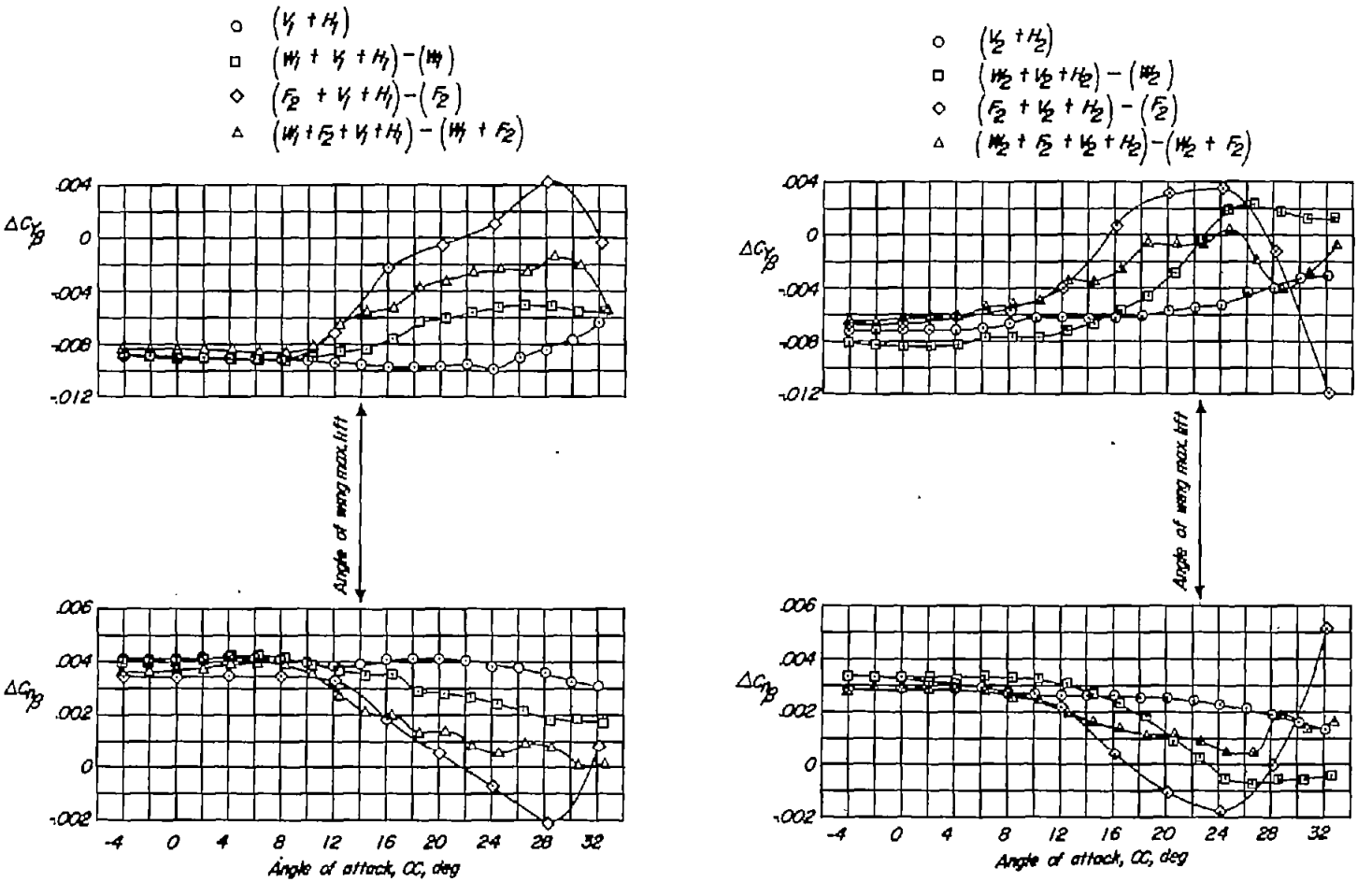

(a) $\Lambda = 0^\circ$.

(b) $\Lambda = 45^\circ$.

Figure 24.- Comparison of the effect of fuselage, wing, and wing-fuselage combination on the tail contribution to C_{Y_β} and C_{n_β}. Fuselage 2.

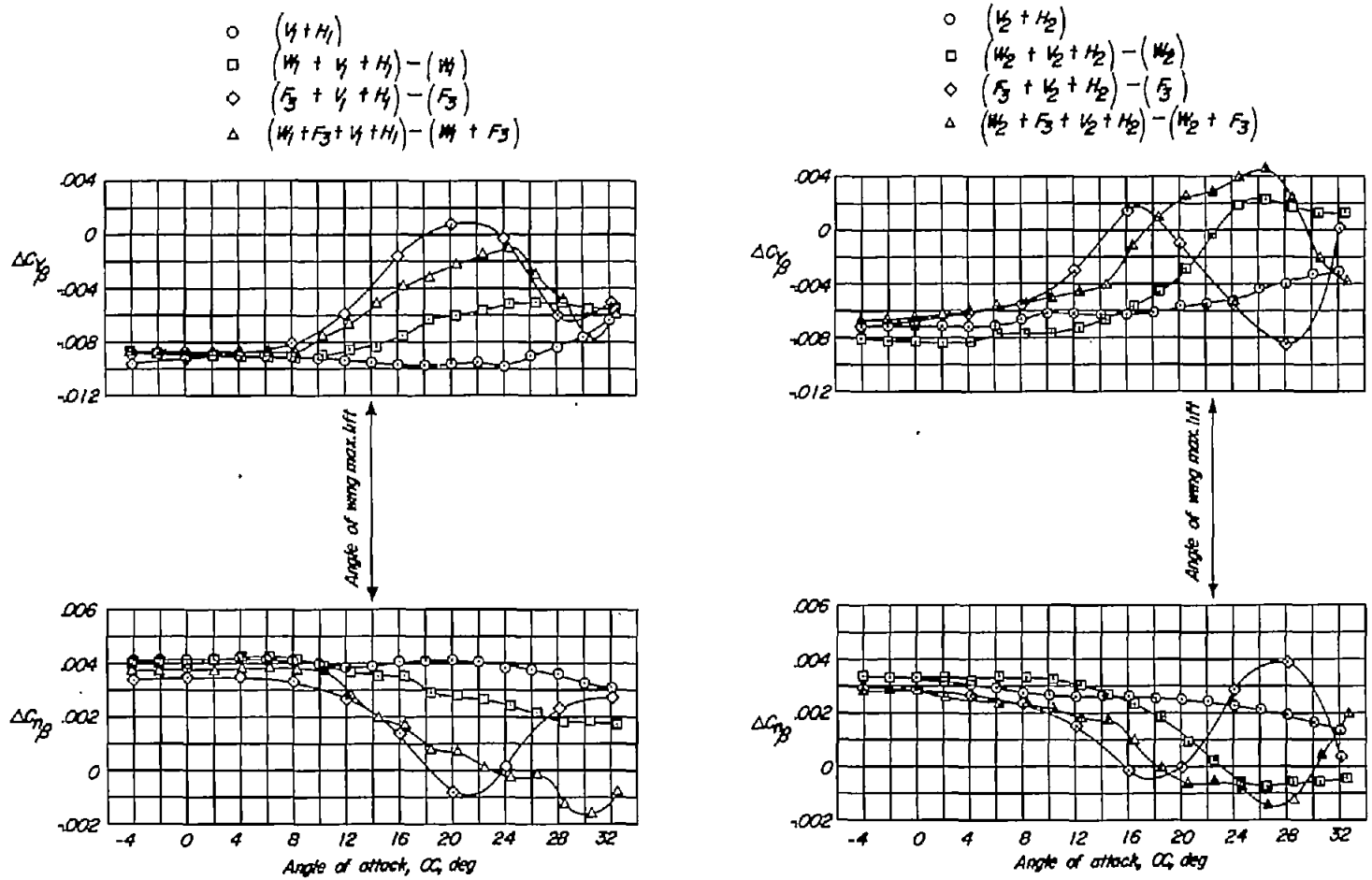

(a) $\Lambda = 0^{\circ}$.

(b) $\Lambda = 45^{\circ}$.

Figure 25.- Comparison of the effect of fuselage, wing, and wing-fuselage combination on the tail contribution to C_{Y_β} and C_{n_β}. Fuselage 3.

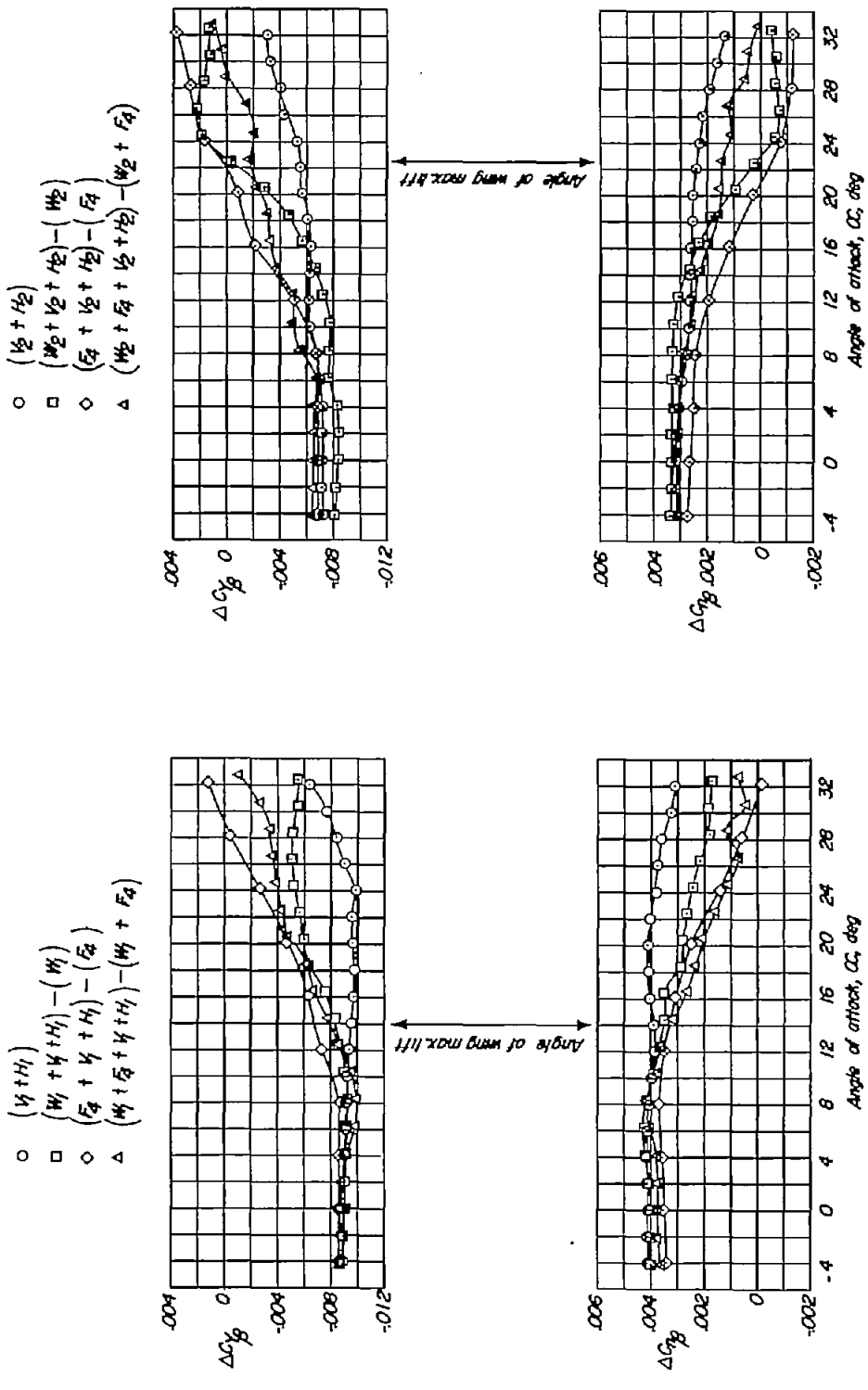

(a) $\Lambda = 0^\circ$.

(b) $\Lambda = 45^\circ$.

Figure 26.- Comparison of the effect of fuselage, wing, and wing-fuselage combination on the tail contribution to C_{Y_β} and C_{n_β}. Fuselage 4.